Mathematical Model to Predict the Solid Airborne Particles Concentration in Occupational Settings

by

Alireza FALLAHFARD

THESIS PRESENTED TO ÉCOLE DE TECHNOLOGIE SUPÉRIEURE
IN PARTIAL FULFILLMENT FOR A MASTER'S DEGREE
WITH THESIS IN MECHANICAL ENGINEERING
M.A. Sc.

MONTREAL, FEBRUARY 28, 2022

ÉCOLE DE TECHNOLOGIE SUPÉRIEURE
UNIVERSITÉ DU QUÉBEC

BOARD OF EXAMINERS

THIS THESIS HAS BEEN EVALUATED

BY THE FOLLOWING BOARD OF EXAMINERS

Mr. Stéphane Hallé, Thesis Supervisor
Department of Mechanical Engineering, École de technologie supérieure

Mr. Ludwig Vinches, Thesis Co-supervisor
School of Public Health
Department of Environmental and Occupational Health, Université de Montréal

Mr. Patrick Germain, President of the Board of Examiners
Department of Mechanical Engineering, École de technologie supérieure

Mr. Lucas Hof, Member of the jury
Department of Mechanical Engineering, École de technologie supérieure

THIS THESIS WAS PRESENTED AND DEFENDED

IN THE PRESENCE OF A BOARD OF EXAMINERS AND PUBLIC

AT ÉCOLE DE TECHNOLOGIE SUPÉRIEURE

ACKNOWLEDGMENT

This master thesis would not be accomplished without the help of people who supported me unlimitedly during my studies. I want to take advantage of this section to share my feelings and thank them.

I would like to say a special thanks to my supervisor, Pr. Halle for his supports, encouragement, advice, and kindness. He was always available to help his students even during the pandemic era and treated them very kindly. He understands international students and their challenges very well and supports them in all situations. Thank you, Pr. Halle, for helping me, grabbing my hands modestly in many hard situations, and showing me the right path. You will always be in my memory as one of the nicest professors that I have ever met.

With many thanks to my co-supervisor, Pr. Vinches, for his kindness, support, and unlimited bits of help. This thesis results from more than two years of his mental and academic support. I am pretty sure that I wouldn't reach this level without his kind advice. He is always a friend more than a supervisor with all students, which eases the pressure of the difficulties. The way that he behaved with me was very pricy, and it meant a lot to me. I hope I could have a chance to compensate for your kindness.

I would like to thank one of the most valuable people in our research group, Dr. Mohammed Zemzem. He played the role of a true brother, best friend, and best colleague through all situations. He always tried to find a way to help me to overcome the hardest moment. Thank you, my brother, for everything. I am incredibly grateful for our friendship and fraternity.

I would like to say thank you to my best friend Afshin Najafi, who kindly covered me and rolled me as a true brother for me here. Thanks to Hossein Savaadkoohian, for all your curing and support without any expectations. Thanks to all colleagues, I have had the chance to meet and share good times: Valérie, Hélène, Elham, Parisa, Negar, Vahid, Iman, Zakaria, Maryam, and 3475 FamilyTeam. A special thanks to Loïc Wingert at IRSST for his sharing the instruments and technical advice.

From the bottom of my heart, I would like to say big thanks to my parents, Mohammad and Talaat, who supported me mentally through this journey and covered me financially despite the many difficulties and limitations that they had. I cannot find a word to say how much I miss them after three years. Thanks to my brothers and sister Abbas, Maryam, and Hamed for all the supports. Words cannot express how much you are valuable to me.

Last and foremost, I want to devote the most especial thanks to my, closest and best friend, my fiancé Madam Saeedeh. Azizam, I cannot find an appropriate word to appreciate your kindness and support. Thanks for standing beside me in the last hard final steps. Thank you for those words and reactions that vanished all the disappointing moments. Merci beaucoup, mon amour, mon trésor, ma merveille, mon tout.

I want to finish this section with a poem from a poet who is from my hometown. The context of this poem is like a light that shows me the way in the darkest moment.

"*Human beings are parts of each other, In creation are indeed of one essence. If one part is afflicted with pain, other parts uneasy will remain. If you have no sympathy for human pain, The name of human you cannot retain."*
-Saadi Shirazi

MODÈLE MATHÉMATIQUE POUR PRÉDIRE LA CONCENTRATION DE PARTICULES SOLIDES EN SUSPENSION DANS L'AIR EN MILIEU PROFESSIONNEL

Alireza FALLAHFARD

RESUME

En milieu de travail, l'exposition aux contaminants présent dans l'air doit être évaluée pour des raisons de santé et de sécurité. Cette évaluation peut être effectuée numériquement ou expérimentalement, mais l'approche numérique peut être utile lorsque les expériences sont difficiles à réaliser. Le modèle « well-mixed room » (WMR) est un modèle numérique simple qui peut prédire les niveaux d'exposition aux contaminants gazeux mais son utilisation pour les aérosols est discutable car il omet des phénomènes importants tels que le dépôt des particules sur les surfaces solides. L'objectif principal de ce mémoire était de déterminer si le dépôt de particules en suspension dans l'air est significatif ou non à l'intérieur d'une petite chambre.

Pour atteindre cet objectif, le modèle standard WMR a été modifié pour prendre en compte le dépôt de particules par déposition gravitationnelle et par diffusion brownienne et turbulente. Trois modèles de dépôt ont également été implémentés dans le modèle. Les concentrations de particules en suspension dans l'air en fonction du temps ont été comparées à des résultats expérimentaux. Les expériences ont été menées dans une chambre de 0,512 m^3 avec des particules de polystyrène de 1, 2 et 3 µm de diamètre et deux niveaux de changement d'air par heure (1,4 et 3,0).

Les résultats numériques ont montré que la différence moyenne entre le taux de dépôt prédit par les trois modèles était inférieure à 2 %. Les résultats expérimentaux et numériques ont été comparés pour une période d'émission de particules et une période sans émission de particules (période de décroissance). Dans la période d'émission, les résultats numériques suivent de près les données expérimentales. Cependant, le modèle WMR modifié surestime considérablement les concentrations expérimentales dans la période de décroissance. Cette constatation est due à une sous-estimation du taux de dépôt dans le modèle. Selon nos paramètres expérimentaux, le dépôt de particules est important mais les mécanismes de dépôt qui ont été pris en compte dans le modèle ne sont pas suffisants pour prédire les taux de déposition. Le rôle d'autres mécanismes de déposition devrait être étudié.

MATHEMATICAL MODEL TO PREDICT THE SOLID AIRBORNE PARTICLES CONCENTRATION IN OCCUPATIONAL SETTINGS

Alireza Fallahfard

ABSTRACT

In the workplace, the contaminant exposure to airborne hazards should be evaluated due to health and safety issues. It can be done numerically or experimentally, but the numerical approach can be useful when challenging to perform experiments. The well-mixed room (WMR) model is a simple model that can predict the exposure levels to gaseous contaminants, but its use for aerosols is questionable since it omits important phenomena such as particle deposition to solid surfaces. The main objective of this master's thesis was to determine whether or not the deposition of airborne particles is significant inside a small chamber.

To reach this objective, the standard WMR model has been modified to consider the deposition of particles by gravitational settling and Brownian and turbulent deposition. Three deposition models were also implemented in the model. The time-dependent concentrations of airborne particles were compared to experimental results. Experiments were conducted in a 0.512 m^3 chamber with polystyrene particles of 1, 2, and 3 μm in diameter and two ventilation air change rates (1.4 and 3.0).

The numerical results showed that the average difference between the predicted deposition rate by the three models was less than 2%. The experimental and numerical results were compared for a particle emission period and a period without particle emission (decay period). In the emission period, the numerical results closely follow the experimental data. However, the modified WMR model overestimate significantly the experimental results in the decay period. This finding is due to an underestimation of the deposition rate in the model. According to our experimental parameters, the particle deposition is significant, but the deposition mechanisms that were considered in the model were not sufficient to predict deposition rates. The role of other removal mechanisms should be investigated.

TABLE OF CONTENTS

LIST OF TABLES

Page

LIST OF FIGURES

Page

LIST OF ABBREVIATIONS

ACH	Air change per hour
CFD	Computational fluid dynamics
DC	Direct current
FDS	Fire dynamic simulator software
FF	Far-field
HEPA	High efficiency particulate air
IRSST	Institut de recherche Robert-Sauvé en santé et en sécurité du travail
LES	Large eddy simulation
NF	Near field
NS	Navier-Stokes
NIST	National Institute of Standards and Technology
OPS	Optical particle counters
REACH	Regulation Registration Evaluation Authorization and Restriction of Chemicals
WMR	Well-mixed room

LIST OF SYMBOLS

A_{dd}	Deposition surface area of downward surfaces (m^2)
A_{du}	Deposition surface area of upward surfaces (m^2)
A_{dv}	Deposition surface area of vertical surfaces (m^2)
C_c	Cunningham correction factor
C_{in}	Inlet concentration (mg/m^3)
C_{out}	Outlet concentration (mg/m^3)
C_{room}	Room concentration (mg/m^3)
D_B	Brownian diffusion coefficient (m^2/s)
d_p	Particle diameter (m)
g	Gravitational acceleration (m/s^2)
G	Contaminant generated rate (mg/min)
I	Integral for deposition velocity of Lai and Nazaroff model
K	Kelvin
k_B	Boltzmann constant (J/K)
Kn	Knudsen number
Q_{in}	Inlet airflow rate (m^3/min)
Q_{out}	Outlet airflow rate (m^3/min)
Re	Reynolds number
Re_p	Reynolds number of a particle
Sc_B	Brownian Schmidt number
T	Temperature (K)
U_m	Fluid flow's velocity (m/s)

u^*	Friction velocity (m/s)
V	Volume (m^3)
v_f	Kinematic viscosity (m^2/s)
v_d^+	Dimensionless deposition velocity
v_{dd}	Deposition velocity on downward surfaces (m/s)
v_{du}	Deposition velocity on upward surfaces (m/s)
v_{dv}	Deposition velocity on vertical surfaces (m/s)
v_{TS}	Terminal settling velocity (m/s)
v_d^+	Dimensionless deposition velocity
β	Particle deposition coefficient (min^{-1})
λ	Mean free path of the gas molecules (m)
ρ_p	Particle density (kg/m^3)
μ_f	Dynamic viscosity of the fluid ($kg/(m \cdot s)$)
τ_p	Particle relaxation time (s)
τ_p^+	Dimensionless particle relaxation time

INTRODUCTION

Aerosols are defined as particles or droplets suspended in a gaseous medium (Hinds,1999). These particles can be generated naturally like soil, soot, or sea salt (Hinds, 1999) or be produced unintentionally by anthropogenic processes such as different industrial activities like mining (Csavina *et al.*, 2012), granite polishing (Saidi *et al.*, 2015), welding (Avino *et al.*, 2015), and other industrial processes (Zuskin *et al.*, 1997).

The airborne particles can penetrate human organs such as lungs due to their small size and deposited on a different section of the respiratory system (Bierkandt *et al.*, 2018). Toxicological studies have shown that short-term and long-term exposure to hazardous can lead to adverse health effects such as cardiovascular diseases, cancer, inflammations, and impaired lung function (Thurston *et al.*, 2017; Butt *et al.*, 2017; Landrigan *et al.*, 2018).

Thus, aerosol release in indoor places is one of the key environmental health and safety issues due to the high risk of contamination (Ribalta, Koivisto, Salmatonidis, *et al.*, 2019). Workplace exposure levels can be 60 to 450 times higher than the residential sector, thus assessing exposure levels in workplaces require a higher level of surveillance (Viitanen *et al.*, 2017).

The evaluation of quantitative exposure levels can be done by experimental measurements or by numerical approaches. The most reliable technique is a well-performed measurement in real-life scenarios (Jensen *et al.*, 2019). However, in real-world environments, direct measurement is not a trivial task due to the presence of workers, access to emission sources, and other constraints such as time and device limitations. Moreover, because the parameters can change over time (emission rate, ventilation, etc.) many measurements are required to find a proper exposure assessment. The analysis of exposure data must also be interpreted appropriately (Jensen *et al.*, 2019). Due to these shortcomings, mathematical models were developed to overcome some of the stated challenges, estimate occupational exposure, and

determine the effectiveness of engineering-control measures such as general ventilation or localized exhaust systems.

Mathematical modelling can be performed by computational fluid dynamics (CFD), zonal models, or spreadsheets, which provide exposure prediction. Under certain conditions, CFD can provide detailed characteristics of the exposure level in time and space. However, the computation time can be significant or even prohibitive, especially in a large indoor environment. Simplified boundary conditions or inadequate assumptions may lead to errors such as exposure underestimation or overestimation. Moreover, CFD software requires adequate spatial discretization and advanced knowledge (Dols, Persily et Polidoro, 2018).

Zonal models, such as the near field/far field (NF/FF) and one-zone model also called well-mixed room (WMR) model, are relatively easy to use and can capture the essence of an exposure scenario to give acceptable estimates of actual exposures according to their criteria. However, most zonal models were developed for gaseous contaminants and do not apply to solid airborne particles. Unlike gas, aerosols can be deposited on the walls and surfaces that lead to surface contamination and a reduction of airborne particle concentration.

The main objective of this master's thesis is to determine experimentally whether or not the deposition of airborne particles is significant inside a small chamber for two different ventilation scenarios.
The sub-objectives are:

1- Compare the measured concentration of airborne particles to the concentration predicted by the one-zone exposure model.
2- Compare the deposition fraction by gravitational settling and Brownian and turbulent deposition of airborne particles for each scenario to the prediction of three deposition models.

This thesis is structured in three chapters: Chapter 1 is devoted to the literature review. It introduces aerosol emission sources in the indoor environment. Then a brief explanation of

aerosol aerodynamic behaviour. After that, the deposition mechanism and its important parameters are presented. Finally, the CFD, two-zone, and one-zone models and their application in other studies are presented.

Chapter 2 presents the numerical methodology and the experimental protocol to achieve the project's objectives. This chapter begins by introducing mathematical expressions for the one-zone model. This chapter presents the mass balance equation for a well-mixed room, deposition coefficient, and the analytic solutions. Then, the experimental setup, measurement devices, and materials are presented. Finally, the experimental study design and the steps of performing the tests are explained.

Chapter 3 is devoted to the results and discussions. The first section presents the tracer gas results and the values of the air change rate in the chamber. In the following, the experimental and numerical results of each scenario are presented. The results are then compared and discussed.

Finally, the thesis finishes with a general conclusion, the limitation of this study, and suggestions for future work.

CHAPTER 1

LITERATURE REVIEW

This chapter introduces a literature review of aerosols in occupational settings. The primary database for the literature review was search engines such as Google scholars, Compendex, Scopus, and ScienceDirect. The general concept of aerosol is vast and crosses several domains such as industrial hygiene, health, mathematics, etc. As a result, the literature review presented in this chapter focused on relevant articles to the objective of this study and does not aim to present a systematic literature review.

The emission sources of aerosols are presented in the first section. In the second section, a brief explanation of aerosol aerodynamic behaviour is presented. After that, the concept of modelling is acquainted.

1.1 Aerosol Emission Sources

The emission sources of aerosols can be categorized as indoor (occupational and residential) and outdoor sources. This section focuses on indoor sources of aerosols in workplaces.

In industrial workplaces, aerosols are generally produced by heating materials, combustion processes, other high temperatures processes, and mechanical processing of materials (Manigrasso *et al.*, 2019). There are many investigations done in various workplaces to identify emission sources and measure aerosol concentration. For instance, Zhang et al. investigated metal arc welding processes in an indoor automotive plant. It revealed that in a welding booth equipped with an exhaust hood, the average concentration of aerosols could easily reach 1.8×10^5 particles·cm^{-3} (Zhang *et al.*, 2013). Buonanno et al. measured the average concentration of aerosols for resistance welding, gas metal arc welding, and oxyacetylene welding at about 3 m from the source operation in an automotive plant. The concentration of aerosols was 1.9×10^5 particles·cm^{-3}, 9.6×10^4 particles·cm^{-3}, and

2.3×10^5 particles·cm^{-3} for resistance welding, gas metal arc welding, and oxyacetylene welding, respectively (Buonanno, Morawska et Stabile, 2011).

Furthermore, in other non-industrial indoor workplaces such as a dental clinic, aerosols can be emitted with a high concentration. In the dental sector, airborne particles can reach concentrations of the order of 1.86×10^5 particles·cm^{-3} to 4.3×10^5 particles·cm^{-3} depending on the type of procedure and treatment (Esteban Florez *et al.*, 2021). Van Landuyt et al. carried out aerosol measurements in a dental workplace. They investigated an abrasive procedure on dental composites. They found that during the grinding, both dental personnel and patients were exposed to the airborne concentration ranging from 5×10^6 to 2×10^7 particles·cm^{-3}. The airborne particle consisted mainly of filler material or resin (Van Landuyt *et al.*, 2014).

1.2 Aerosols aerodynamic behavior

The concept of aerosol aerodynamic behaviour and its fundamental is a vast subject. This subject is briefly presented in this section and focuses on related items to this study.

A significant number of particles can be discharged into the environment after aerosols are released from any source. These particles can be transported through the ambient air due to diffusion, advection, and external forces. They move in the opposite direction of the concentration gradient, namely from places with higher concentrations into lower concentrations due to Brownian and turbulent diffusion. Moreover, particles move with fluid flow due to advection. Through their transportation, some phenomena such as coagulation and deposition may occur.

Particles may collide with each other through their transport due to the relative motion of particles or external forces (Kulkarni, Baron et Willeke, 2011). After the collision, they merge and form a larger particle by coagulation process (Hinds, 1999). In the case of solid particles, the process is called agglomeration, and the resulting particles are known as agglomerated particles (Hinds, 1999). Coagulation or agglomeration leads to a decrease in particle number

and increases in particle size. In the indoor environment, coagulation becomes significant when the number concentration typically exceeds $\approx 10^5$ particles·cm^{-3} (Hussein et al. 2009; Chatoutsidou et al. 2017).

A portion of particles may be deposited on solid walls or boundaries through their displacement, which refers to the particle disposition (Minier et Pozorski, 2017). The deposition of particles occurs due to five mechanisms: gravitational settling, Brownian and turbulent diffusion, electrostatic deposition, and thermophoresis. Gravitational settling occurs when the gravitational force is significant in comparison with other forces, and particles settle due to gravity forces (Lai et Nazaroff, 2000). Particles may be deposited on surfaces by their random motion due to Brownian diffusion. Indoor air flows generated by ventilation are generally turbulent. Turbulent eddies in the air can lead the particles to collide with the surfaces and deposit on them. This phenomenon is known as a turbulent deposition. Electrostatic deposition occurs to the highly charged particles or unipolar charged aerosols due to their repulse that drives particles away from each other and deposited on the surface (Fan et Ahmadi, 1994 ; Hidy, 2012 ; Soltani et Ahmadi, 1999). The thermophoresis deposition occurs in the presence of a temperature gradient between a surface and the environment. This mechanism leads the particles to migrate in the opposite direction of the temperature gradient (Zahmatkesh, 2008 ; Changfu et Guanghui, 2008). In a typical indoor environment without a significant temperature gradient, gravitational settling and turbulent deposition are generally the two main deposition mechanisms. To better understand these two deposition mechanisms, the following subsection is devoted to presenting some of the fundamental parameters related to particle deposition, such as particle flow regime, the relaxation time of particles, deposition regime, and deposition velocity.

1.2.1 Particle deposition parameters

Understanding aerosol deposition requires knowing important physical concepts of fluid flow in which particles are suspended, the interaction of the particles with the surrounding gas, and the deposition velocity of particles on surfaces.

The aerosol particles constantly collide with a great number of surrounding gas molecules. As a reminder, the mean free path (λ) is an average distance over which a gas molecule travels between two consecutive collisions. At standard pressure and temperature λ ≅ 67 nm. If the particle diameter (d_p) is much larger than the mean free path of the gas molecules, the flow can be recognized as a continuum flow regime. If the diameter of the particles is much lower than the λ, the particles slip through the vacuums between the gas molecules before colliding with them. The flow regime identification can be determined by a dimensionless number called the Knudsen number, Kn (Table 1.1). Kn << 1 indicates the continuum flow regime, and Kn >> 1 indicates the free molecular flow regime. For the intermediate range, 0.4 <Kn <20 is referred to as the slip flow regime (Kulkarni, Baron et Willeke, 2011).

Stokes derived an expression for determining the terminal settling velocity (v_{TS}) for a particle due to gravitational settling, which is recognized as Stokes law. The main assumption of this law is assuming that the inertia forces are much smaller than viscous forces. This assumption can be checked by determining the value of a dimensionless number called particle Reynolds number (Re_p). The Reynolds number for a particle determines the ratio of inertial forces and viscous forces, as presented in Table 1.1. When $Re_p < 1$, the inertial forces are much smaller than the viscous forces. This regime is called Stokes's regime, and Stokes's law applies to the particle within this regime.

However, in the slip regime, slipping of the particles through the gas molecule leads to increased particle velocity compared to the predicted Stokes's velocity. This difference accommodates by the slip correction factor, also called the Cunningham correction factor (C_c).

The particle deposition velocity depends on the deposition regime. Particle deposition regime includes three regimes: 1) diffusion, 2) diffusion-impaction and 3) inertia-moderated. The identification of the deposition regime for the particle is determined by the dimensionless particle relaxation time (τ_p^+). τ_p^+ depends on the relaxation time, the time that particle's velocity adjusts to flow velocity, and friction velocity u^*. The value of dimensionless particle dimensionless relaxation time for diffusion regime is $\tau_p^+ < 0.1$, diffusion-impaction regime is

$0.1 < \tau_p^+ < 10$ and inertia-moderated regime occurs for $\tau_p^+ > 10$. The importance of diffusion is presented by the Schmidt number (Sc_B) that determined the ratio of kinematic viscosity (v_f) and particle diffusivity (D_B). Table 1.1 present the mentioned parameters, their mathematical expression, and the units of each variable.

Table 1.1 Required parameters for deposition

$Kn = \frac{\lambda}{d_p}$	Kn: Knudsen number λ: Mean free path of the gas molecules (m) d_p: Particle diameter (m)
$Re_p = \frac{U_m \cdot d_p}{v_f}$	Re_p: Reynolds number of a particle U_m : Fluid flow's velocity (m/s) v_f: Kinematic viscosity (m^2/s)
$v_{TS} = \frac{{d_p}^2 \cdot \rho_p \cdot g \cdot C_c}{18 \cdot \mu_f}$	v_{TS}: Terminal settling velocity (m/s) ρ_p: Particle density (kg/m^3) g: Gravitational acceleration (m/s^2) μ_f: Dynamic viscosity of the fluid [kg/(m · s)]
$C_c = 1 + \frac{\lambda}{d_p} \cdot \left[2.34 + 1.05 \cdot e^{\left(-0.39 \cdot \frac{\lambda}{d_p}\right)}\right]$	C_c: Cunningham correction factor
$\tau_p = \frac{{d_p}^2 \cdot \rho_p \cdot C_c}{18 \cdot \mu_f}$	τ_p: Particle relaxation time (s)
$\tau_p^+ = \frac{\tau_p \cdot u^{*2}}{v_f}$	τ_p^+: Dimensionless particle relaxation time u^*: Friction velocity (m/s)
$D_B = \frac{k_B \cdot T \cdot C_c}{3\pi \cdot \mu_f \cdot d_p}$	D_B: Brownian diffusion coefficient (m^2/s) k_B: Boltzmann constant (J/K) T: Temperature (K)
$Sc_B = \frac{v_f}{D_B}$	Sc_B: Brownian Schmidt number

Several correlations were developed to estimate the deposition velocity. The correlations were obtained by performing experiments to assess the deposition of particles on the walls in simple geometries. Although relatively old, the correlations are still used as a benchmark in many studies. Table 1.2 presents some of them.

Table 1.2 Deposition velocity on surfaces

Deposition velocity by Brownian and turbulent diffusion on vertical surfaces (v_{dv}) ($\tau_p^+ < 0.1$)		
Type: $v_d^+ = k_1 Sc_B^{\alpha}, \alpha = -\frac{2}{3}$ ($v_d^+ = \frac{v_{dv}}{u^*}$)	$v_d^+ = 0.084 Sc_B^{-\frac{2}{3}}$	Cleaver et Yates, 1975
	$v_d^+ = 0.059 Sc_B^{-\frac{2}{3}}$	Friedlander, 1977
	$v_d^+ = 0.045 Sc_B^{-\frac{2}{3}}$	Wood, 1981
	$v_d^+ = 0.075 Sc_B^{-\frac{2}{3}}$	Davies, 1983
	$v_d^+ = 0.07 Sc_B^{-\frac{2}{3}}$	Papavergos et Hedley, 1984
	$v_d^+ = 0.061 Sc_B^{-\frac{2}{3}}$	Shimada et al., 1993
Type: $v_d^+ = k_1 Sc_B^{\alpha}, \alpha \neq -\frac{2}{3}$ ($v_d^+ = \frac{v_{dv}}{u^*}$)	$v_d^+ = 0.0889 Sc_B^{-0.704}$	Shaw and Hanratty, 1977
	$v_d^+ = 0.13337 Sc_B^{-0.75}$	Levich, 1962
	$v_d^+ = 0.123 Sc_B^{-0.75}$	Charurau, 1982
$v_{dv} = \frac{u^*}{I}$ $I = [3.64 \cdot Sc_B^{\frac{2}{3}} \cdot (\mathrm{a} - \mathrm{b}) + 39], d_p > 0.01\mu m$ $\mathrm{a} = \frac{1}{2} \cdot \ln\left[\frac{\left(10.92 \cdot Sc_B^{-\frac{1}{3}} + 4.3\right)^3}{Sc_B^{-1} + 0.0609}\right] + \sqrt{3} \cdot tan^{-1}\left[\frac{8.6 - 10.92 \cdot Sc_B^{-\frac{1}{3}}}{\sqrt{3} \cdot 10.92 \cdot Sc_B^{-\frac{1}{3}}}\right]$ $\mathrm{b} = \frac{1}{2} \cdot \ln\left[\frac{\left(10.92 Sc_B^{-\frac{1}{3}} + r^+\right)^3}{Sc_B^{-1} + 7.699 \times 10^{-4}(r^+)^3}\right] + \sqrt{3} \cdot tan^{-1}\left[\frac{2r^+ - 10.92 Sc_B^{-\frac{1}{3}}}{\sqrt{3} \cdot 10.92 Sc_B^{-\frac{1}{3}}}\right]$ $r^+ = \frac{d_p \cdot u^*}{2 \cdot v_f}$		Lai and Nazaroff, 2000
Deposition on horizontal surfaces ($\tau_p^+ < 0.1$)		
Upward surfaces (v_{du})	$v_{du} = \frac{v_{TS}}{1 - \exp\left(-\frac{v_{TS} \cdot \mathrm{I}}{u^*}\right)}$	Lai and Nazaroff, 2000
Downward surfaces (v_{dd})	$v_{dd} = \frac{v_{TS}}{\exp\left(\frac{v_{TS} \cdot \mathrm{I}}{u^*}\right) - 1}$	

1.3 Models and Modelling

A model is a simplified version of a system in a real condition, and the purpose of modelling is to represent how a system works or responds to the changes in the system's inputs. The industrial hygienist uses statistical and mathematical models to describe the relationships between the level of exposure and factors determining or affecting exposures. Moreover, several official organizations, such as Regulation Registration Evaluation Authorization and Restriction of Chemicals (REACH) in the European Union and the Institut de recherche Robert-Sauvé en santé et en sécurité du travail (IRSST), highly recommend using modelling to assess occupational exposure to chemical products. It is worth mentioning that using models is not intended to replace direct measurements. A modelling approach supports the decision process on the air sampling when the exposure assessment is not possible such as scenarios that cannot be verified experimentally: accidents, a large spill of contaminants, a breakdown of the ventilation system, etc. (Keil, Cimmons et Anthony, 2009). Mathematical modelling can be done by models with varying complexity. Models such as one–zone or two-zones are considered simple. In contrast, models based on the resolution of the Navier-Stokes equations are more complex, but they allow a detailed description of the aerodynamic behaviour of aerosols.

1.3.1 CFD Models

CFD models are based on fundamental conservation laws that govern fluid movement and contaminants transport in a spatial and temporal framework. CFD determines the fluid flow numerically by solving approximately the non-linear differential equations that govern the fluid flow. In industrial hygiene engineering, CFD models have been used to study the air movement and evaluate the transport of gaseous and particulate contaminants associated with ventilation and engineering control. CFD modelling is frequently used to predict aerosol dynamic behaviour and contaminant transport. For example, Lui et al. utilized a CFD approach to predict the particle deposition velocity in enclosed spaces under natural ventilation in three typical rooms: Z-type, L-type, and rectangle types (Liu *et al.*, 2019). Another illustration is the

prediction of a particle deposition inside the airplane cabin by Cao et al. (Cao *et al.*, 2018). CFD tools provide many benefits for the user while they have their drawbacks. The complexity and the time required to create the computational domain with accurate discretization and running the simulation may take days or weeks are the main disadvantages of CFD tools (Ribalta *et al.*, 2019 ; Wu *et al.*, 2010 ; van Hooff et Blocken, 2012 ; Ha et Choe, 2014). Moreover, most CFD codes are not accessible to the public, and commercial codes are expensive.

1.3.2 Zonal Models

Zonal models such as the two-zone model (near-field/far-field) and one zone model, also called well-mixed room (WMR) model, are among the simple mathematical prediction models that have been proved as a practical tool in occupational exposure assessment (Arnold, Shao et Ramachandran, 2017). In the two-zone model, the room splits into two zones with uniform air mixing in each zone. The first zone is near the contaminant emission source (near field), and the second zone (far field) is the remainder of the room (Keil, Cimmons et Anthony, 2009). The contaminant transport between these two zones is done by an inter-zonal air flow rate that accounts for the near-field geometry and local airspeed. For determining the contaminant concentration, the mass balance equation is applied for each zone.

The main challenges in the two-zone model are the choice of an appropriate geometry for the near field in a given exposure scenario. There is no clear guideline for the size and geometry of the near field and estimating the interface velocity between the NF-FF. In case of facing reviewed the challenge of the two-zone model, a simpler model can be used. The simpler model focused in this study is one of the most often used, and this model is the WMR model, also called the one-box model (Keil, Cimmons et Anthony, 2009).

This model considers the whole volume of the room as one zone. The main assumption is that the air inside the room is well-mixed, which implies a uniform concentration. For finding the concentration with time inside the room, a mass balance equation is applied. The mass balance

equation for the one-zone model and mathematical aspect are presented and explained in chapter 2. In this section, the model background and some previous studies are presented.

This model was initially proposed by Jayjock (Jayjock, 1997) and applied in many research studies, as illustrated in the following text. Arnold et al. performed a series of chamber studies to evaluate the performance of the WMR model under controlled conditions that were changed systematically (Arnold, Shao et Ramachandran, 2017). For this study, they used three solvents frequently used in industry: acetone, toluene, and 2-butanone. Solvents were injected into the chamber under three different generation rates (0.05 $mL \cdot min^{-1}$, 0.1 $mL \cdot min^{-1,}$ and 0.15 $mL \cdot min^{-1}$) via Harvard Apparatus Pump equipped with 50 mL glass syringes. Then, the solvents evaporated immediately upon injection into the chamber. Three ventilation rates are considered for the chamber (0.055 $m^3 \cdot min^{-1}$, 0.25 $m^3 \cdot min^{-1}$, and 0.62 $m^3 \cdot min^{-1}$). Concurrently, solvent vapour concentrations are measured at 6 locations across the chamber. Finally, they compared the measured and predicted concentrations by using the criteria of ASTM standard 5157 (ASTM Committee D22, 2019). According to their evaluation criteria, their prediction, and experimental results are in agreement with 97% for the acetone tests, 96% for the toluene tests, and 88% for the 2-butanone tests.

Ribalta et al. applied the WMR to evaluate the model's performance in two thermal spraying booths (Ribalta, Koivisto, Salmatonidis, *et al.*, 2019). The first booth had a volume of 465 m^3 and 35 air change per hour (ACH), and the second booth's volume was 250 m^3 with 25 ACH. They measured the aerosol concentration during the thermal spraying of ceramic coatings. Meanwhile, the WMR model is used to estimate the concentration inside the booths and compared the results with the observed concentration. Their findings reveal that the predicted concentration was 0.2 to 0.7 times the measured concentration. Despite this underestimation of the concentrations, they announced that WMR models could provide practical suggestions on the order of magnitude of predicted particle number concentrations in industrial settings when properly parameterized and utilized as a preliminary risk assessment tool.

Finally, a recent analysis of the WMR model was done by Arnold et al. (Arnold *et al.*, 2020). They applied aqueous acetic acid on the surfaces of three rooms with the ACH of 1.22, 1.6, and 3.4. The concentration of evaporated acetic acid is measured directly and estimated by the WMR model. The comparison of model and measurement results reveals a 95% confidence interval between the model result and the experimental data.

CHAPTER 2

METHODOLOGY

This chapter presents the methodology for mathematical modelling and experimental protocol to achieve the objectives of the project. This chapter begins by introducing mathematical expressions for the one-zone model. In this section, the mass balance equation for a well-mixed room, deposition coefficient, and the analytic solutions are presented, and the physical meaning of each term is explained. Then, the experimental setup, such as the chamber configuration, measurement devices, and materials, are presented. Finally, the experimental design and the steps required to perform the tests are explained.

2.1 Analytic Model

The traditional WMR model for gaseous contaminants is the base of the proposed model for this study. This model can predict the contaminant concentration in indoor environments with a well-mixed air hypothesis. In other terms, the main assumption of this model is the well-mixed condition which allows us to neglect the concentration gradient in an indoor environment.

In this model, the airflow goes into the room with the volume flow rate of Q_{in} in m^3/min. The mass concentration of gaseous contaminants in the inlet flow is C_{in} in mg/m^3. The contaminant is generated from a source with the rate of G (mg/min) inside the room. A fan provides a well-mixed condition, and the contaminant concentration inside the room is represented only by a scalar quantity: C_{room} in mg/m^3. This concentration is time-dependent. The outlet flow is represented by Q_{out} in m^3/min. Finally, the mass concentration of the gaseous contaminant that leaves the room is C_{out} in mg/m^3. In the WMR model, the outlet concentration is identical to the room concentration $C_{outlet}=C_{room}$ because of the uniform concentration caused by the well-mixed condition. The one-zone concept with the well-mixed hypothesis is schematically presented in Figure 2.1.

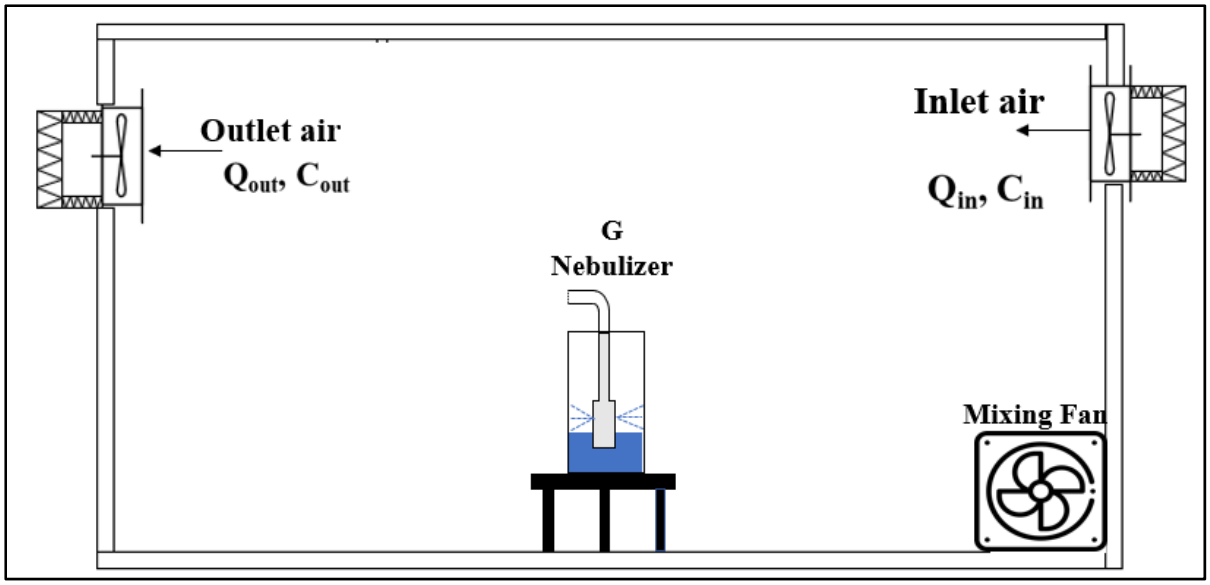

Figure 2.1 Schematic view of WMR model for a well-mixed room

The mass conservation law can be applied to determine the contaminant concentration (C_{room}) as presented in equation 2.1.

$$\dot{Mass}_{accumulated} = \dot{Mass}_{generated} + \dot{Mass}_{in} - \dot{Mass}_{out} \quad (2.1)$$

$$(\boldsymbol{I}) \qquad (\boldsymbol{II}) \qquad (\boldsymbol{III}) \qquad (\boldsymbol{IV})$$

Rate of mass accumulation in the room	Rate of mass-generated from the source	Rate of incoming mass	Rate of leaving mass

Each term of equation (2.1) can be developed in its differential form. The first term (I) represents the rate of contaminants mass accumulation inside a room, and the differential form is equal to $\dot{Mass}_{accumulated} = V \cdot \frac{dC_{room}}{dt}$. The right-hand side of the equation represents the generated contaminant mass rate from a source inside the room (term II), $\dot{Mass}_{generated} = G$, and the contaminant mass entry rate (term III) to the room is $\dot{Mass}_{in} = Q \cdot C_{in}$. The last term (IV) is the rate of contaminant mass leaving the room and is equal to $\dot{Mass}_{out} = Q \cdot C_{out}$. By

substitution of these mathematical equivalents in equation 2.1, we obtain a linear first-order ordinary differential equation:

$$V \cdot \frac{dC_{room}}{dt} = G + Q \cdot C_{in} - Q \cdot C_{out} \quad (2.2)$$

The traditional WMR model was initially developed for gaseous contaminants. In that case, the ventilation (Q) is the only removal mechanism. This equation can be used as a starting point to determine the concentration of solid airborne particles under the WMR assumptions. However, the removal mechanisms are more complex for airborne particles since they are subjected to other physical phenomena such as coagulation and different mechanisms such as thermophoresis, electrostatic and gravitational deposition.

Thus, a term must be added to Eq (2.1) to include the mentioned airborne removal mechanisms. This study focuses on gravitational settling, Brownian and turbulent deposition among different removal mechanisms. Other removal mechanisms such as coagulation, thermophoresis, and electrostatic deposition are neglected for the following reason. Coagulation is neglected because this study focuses on locations where the number concentration of particles is "small". Practically speaking, a number concentration of 10^5 particles·cm^{-3} or less leads to negligible coagulation (Hussein et al. 2009; Chatoutsidou et al. 2017). Moreover, considering coagulation mechanisms increase the mathematical complexity of the model and limit the model to knowledgeable users, which is not aligned with the aim of this master project.

The thermophoresis deposition is neglected because, in the most indoor environment, there is no significant temperature gradient between the surfaces and the environment. The electrostatic deposition is also neglected because quantifying the electrostatic charges on surfaces is not a trivial task. Thus, the two remaining deposition mechanisms are i) the gravitational settling and ii) the deposition by diffusion (Brownian and turbulent).

The gravitational settling and Brownian and turbulent deposition are two important deposition mechanisms in terms of occupational hygiene. Firstly, these two mechanisms cause surface contamination that can lead to skin absorption and occupational diseases such as irritant contact dermatitis, skin cancer, and other miscellaneous skin diseases (NIOSH, 2013). Secondly, particle deposition can significantly change the airborne concentration of aerosols. The mathematical term that presents these two mechanisms can be implemented in the fourth term (IV) of equation 2.1 by adding a coefficient for particle deposition. The fourth term becomes $\dot{Mass}_{out} = Q \cdot C_{out} + \beta \cdot V \cdot C_{room}$ where β is the deposition coefficient ($\min^{-1}$). By considering this, equation 2.2 can be rewritten as:

$$V \cdot \frac{dC_{room}}{dt} = G + Q \cdot C_{in} - Q \cdot C_{out} - \beta \cdot V \cdot C_{room} \tag{2.3}$$

This differential equation governs the concentration of airborne particles as a function of time in a well-mixed environment subject to the assumptions previously made. The mathematical calculation of β is explained in the following subsection. An analytical solution to this equation can be found by assuming a Dirichlet initial condition $C(t = 0) = C_0$ as the background particle concentration. The final analytical solution of equation 2.3 is:

$$C(t) = e^{\left(-\frac{Q}{V}-\beta\right)\times t} \times \left[C_0 - \frac{G + Q \times C_{in}}{\beta \times V + Q}\right] + \frac{G + Q \times C_{in}}{\beta \times V + Q} \tag{2.4}$$

This analytical solution makes it possible to determine the particle concentration inside a WMR. This solution is coded in MATLAB software to predict the particle concentration as a function of time for an indoor environment.

2.1.1 Deposition coefficient

The deposition coefficient (β) can be determined mathematically by (Lai et Nazaroff, 2000):

$$\beta = 60 \cdot \frac{v_{du} \cdot A_{du} + v_{dd} \cdot A_{dd} + v_{dv} \cdot A_{dv}}{V} \tag{2.5}$$

The term V is room volume (m^3) terms v_{du}, v_{dd} and v_{dv} are deposition velocity (m/s), and A_{du}, A_{dd} and A_{dv} are deposition surface area (m^2) for upward, downward, and vertical surfaces, respectively. The method for determining the deposition velocity is explained in the following paragraph.

The first step of determining the deposition velocity for calculating β is to identify the deposition regime and check whether the particle is in the Stokes regime or not. As mentioned in the previous chapter, the value of dimensionless relaxation time and Reynolds number is required to identify the deposition and the Stokes regime. To have these values, some mathematical calculations are performed for three particle diameters 1 μm, 2 μm, and 3 μm at standard temperature and pressure conditions. Table 2.1 presents the key parameters to determine the deposition regime. The reason for choosing these three particle sizes relates to the limitation of the particle generation devices presented in section 2.2.

Table 2.1 Calculations for identifying the deposition regime and being in Stokes's regime

d_p (m)	ρ_p (kg $\cdot m^{-3}$)	Re_p	C_c	V_{TS} (m$\cdot s^{-1}$)	τ_p(s)	τ_p^+
1.00E-06	1050	6.62E-04	1.15	3.61E-05	3.68E-06	2.44E-05
2.00E-06	1050	1.32E-03	1.07	1.35E-04	1.37E-05	9.11E-05
3.00E-06	1050	1.99E-03	1.05	2.97E-04	3.02E-05	2.00E-04

As can be seen, the value of the Re_p is less than 1, and it confirms that the particles are in the Stokes regime, and Stokes's law is applicable for the particles. The dimensionless relaxation

time for all the particles is well below 0.1, which means the particles are in the diffusion regime.

The deposition velocity of a particle on vertical and horizontal surfaces for diffusion regime is presented in Table 1.2. For the deposition velocity on horizontal surfaces, the only candidate presented in Table 1.2 is chosen: Lai and Nazaroff 2000. To determine the deposition velocity on vertical surfaces in the diffusion regime, three correlations among the model presented in Table 1.2 are considered for the vertical surfaces: Wood 1981, Charurau 1982, and Lai and Nazaroff 2000.

These relations are selected because they respect the constraint of the relaxation time of the particle. Moreover, there are two types of deposition velocity depending on the power of Schmidt number, and for each type, a representative correlation was chosen. Wood correlation is valid for particles from 0.01 µm to 50 µm, and the Charurau correlation applies for 0.01 µm to 10 µm. Both correlation range is fitted with a range of particle size in this project. The third correlation, Lai and Nazarof, is one of the models which is tested by many studies and one of the most frequently used correlations and applied in many studies and applicable for the chosen particle size (Ribalta *et al.*, 2021 ; Agarwal *et al.*, 2021). These three correlations require the friction velocity value, which is determined from CFD simulations of the airflow inside the chamber under investigation.

2.1.2 CFD simulations

The CFD simulations are performed to characterize the airflow inside the chamber via the open source software Fire Dynamic Simulator (FDS V. 6.7.6) (McGrattan *et al.*, 2021). FDS was developed by the National Institute of Standards and Technology in collaboration with the Technical Research Center of Finland. This software solves the Navier Stokes equations in transient regime on a structured mesh by the large eddy simulation (LES) technique or direct numerical simulation (DNS) technique. The CFD simulation in this study is only used to determine the friction velocity, and focusing on other aspects, and other results was not the

aim of the simulation. The governing equations, mesh independence study, and the mean friction velocity formula are presented in Annex I.

2.2 Experimental setup

All the experiments and indoor sampling are conducted in a parallelepiped Plexiglas chamber measuring 0.750 m (length) × 1.186 m (width) × 0.576 m (height) corresponding to a volume (V) of 0.512 m^3.

2.2.1 Chamber ventilation

The chamber ventilation is supplied by two brushless fans implemented in the chamber's inlet and outlet and joint with high efficiency particulate air (HEPA) filters. Fans are connected to a direct current (DC) power supply to provide various airflow by changing its voltage.

Inside the chamber, a mixing fan is placed to provide well-mixed conditions. Moreover, a rectangular pierced plate (0.10 m ×0.10 m) is implanted in front of the chamber inlet to prevent a direct stream of airflow between the inlet and outlet and obtain a better flow distribution.

The ACH of the chamber is determined by the tracer gas decay method. For each ACH, three tests are performed using three indoor air quality (IAQ) meters (TSI 7525 model) to measure the CO_2 concentration at each second inside the chamber. IAQ meters operate in the concentration range of 0 ppm to 5000 ppm with an uncertainty of 50 ppm or ± 3.0%, which error is greater. One of the devices is mounted near the outlet of the chamber, and two others are located almost in the centreline of the chamber (Figure 2.2).

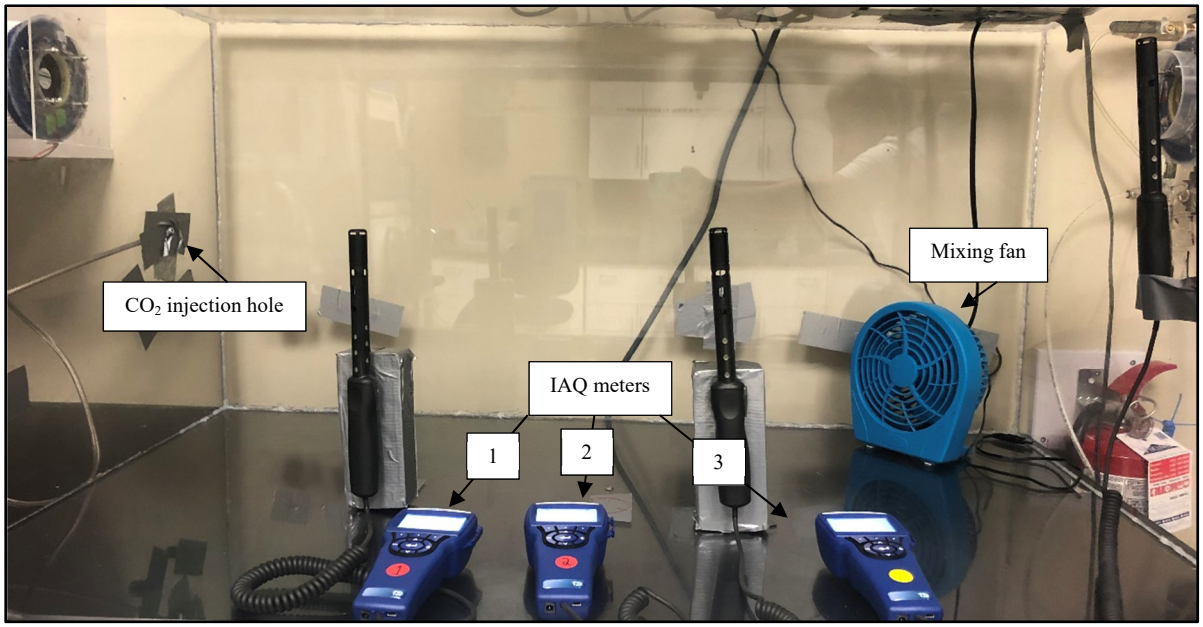

Figure 2.2 Chamber's configuration for tracer gas tests

Before starting the CO_2 tests, all devices' time synchronized. As the first step, all devices measure the background CO_2 concentration before performing each test. Then the CO_2 is injected for two or three seconds via a small injection hole on the chamber's wall. The decay measurements are carried out until the CO_2 concentrations reach the background concentration. The extracted results from the decay of CO_2 concentrations inside the chamber are used to determine the ACH and check the well-mixed condition. The ACH can be calculated by $ACH = \frac{3600 \cdot Q}{V}$ where Q is the ventilation rate (in m^3/s) and V space volume (in m^3). The ventilation rate can be determined by decay concentration of CO_2 using Eq (2.6):

$$-\ln\left(\frac{C_{room,t}}{C_{room,0}}\right) = \frac{Q}{V} \cdot \Delta t \tag{2.6}$$

Where the $C_{room,t}$ is the CO_2 concentration at time t and $C_{room,0}$ is the initial CO_2 concentration at time t_0. The results obtained from the CO_2 tests are presented in the next chapter. The last 3 minutes of the decay test are not considered in Δt since, in this period, the concentration as a function of time is no longer exponential.

2.2.2 Materials and particle counter devices

The particles diameters used for this study are 1, 2, and 3 µm non-functionalized polystyrene microspheres from Polysciences Inc. There are three main reasons for selecting these particles. The first reason is that these particles are low-hazard particles (Robinson *et al.*, 2006), and the second reason is that the particles are well-spherical and in the diffusion regime, as shown in Table 2.1. Thirdly, these particles respect the particle generator size limitation presented in the following paragraphs.

The particles are suspended in deionized water with a concentration of 4.55×10^{10} particles/ml, 5.68×10^{9} particles/ml, and 1.68×10^{9} particles/ml for 1 µm, 2 µm, and 3 µm particles, respectively. The stock solutions are highly concentrated and need to be diluted because these concentrations are well above the range of particles counter devices. These particles are diluted in ultra-pure water (with a resistivity of 18.2 MΩ·cm at 25ºC) to have 0.02% v/v solution. To reduce the agglomeration, the stock solution and final dilution are sonicated for 10 minutes and 25 minutes, respectively.

For generating the particles inside the chamber, a three-jet collision nebulizer manufactured by BGI was employed. The nebulizer was connected to pure air with an inlet pressure of 15 psi. This device is limited to generating particles with a maximum diameter of 3 µm, and selected particles respect this limitation.

The concentration of particles inside the chamber is determined with an optical particle counter (OPS) GT-526S (MetOne Instruments Inc.). This OPS has six channels and can count the particle with an optical diameter of 0.3 µm to 10 µm and accuracy of ± 10%. It should be noted that this device measures the optical diameter and not the aerodynamic diameter. The optical diameter and aerodynamic diameter, the diameter of a sphere of unit density which behaves aerodynamically the same as the particle of the test substance, of the polystyrene particles are almost similar because they are well-spherical particles, and their density is nearly 1000 kg/m^3 (Kulkarni, Baron et Willeke, 2011).

To evaluate the device's performance and reliability, the GT-526S was compared with a well-known OPS TSI 3330 devices and tested at Institut de recherche Robert-Sauvé en santé et en sécurité du travail (IRSST). The details of both device comparisons are presented in Annex II.

The OPS is placed inside the chamber near the source term during the experiment, as presented in Figure 2.3.

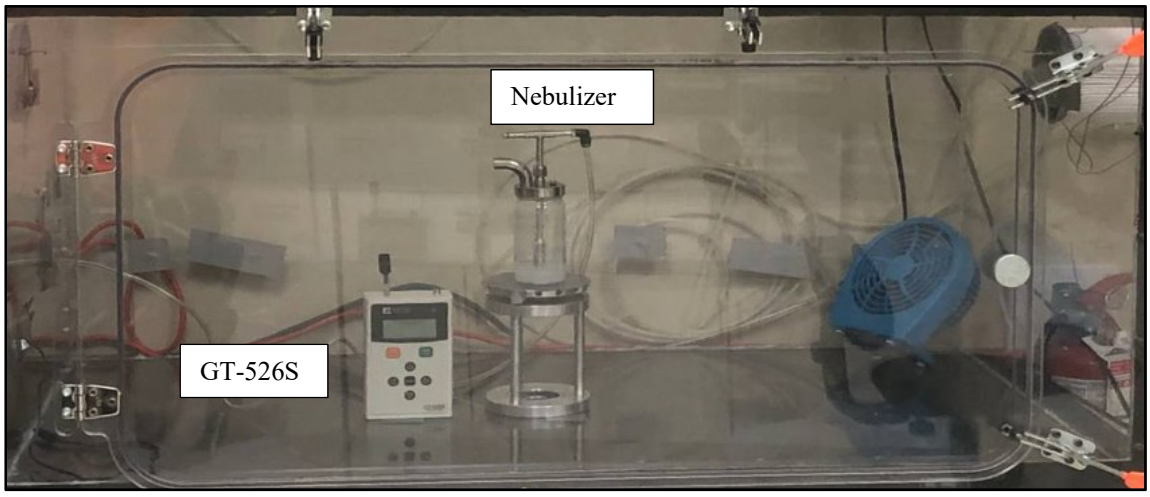

Figure 2.3 Equipped chamber with OPS and nebulizer

2.2.3 Source characterization

Characterizing the source term and estimating the generation rate of the particles are the main challenges in exposure measurements and have been mentioned in many previous studies (Ribalta, Koivisto, Salmatonidis, *et al.*, 2019 ; Ribalta *et al.*, 2021). Generation rate is one of the terms in equation 2.4 and directly affects the predicted concentration by the model. In this study, the generation rate is estimated by measuring the weight of the dilution before and after the experiment by Sartorius ENTRIS balance with the uncertainty of ± 0.002 g. This measurement is used to determine the generation rate, which is explained in the next chapter. Furthermore, the source characterization is achieved by analyzing the output size distribution of the nebulizer during the generation period, and the results are presented in the next chapter.

2.3 Experimental scenarios

The experiments are designed to evaluate the mathematical model in various conditions that are representative of the real-world environment. As mentioned in the previous section, three particle sizes are selected to check these particles' model performance and deposition in each condition. The experiments were carried out for two ventilation flow rates corresponding to 1.4 and 3 ACH. These ACH can be observed in indoor environments. Consequently, six scenarios are planned, i.e., three-particle size and two ventilation rates (Table 2.2).

Table 2.2 The scenarios of experiments

Scenarios	ACH	Particle Size (μm)
1	1.4	1
2	1.4	2
3	1.4	3
4	3	1
5	3	2
6	3	3

Firstly, as a summary of the procedure of the experiment, the chamber is cleaned with wet wipes and alcohol before each experiment and flushed with airflow provided by fans. Secondly, the fans are set to provide the chosen ACH, and the mixing fan is turned on. Thirdly, the background concentration is measured 10 minutes before the particle generation. It is important to know the background concentration (C_0) because it is one of the input parameters in equation 2.4. Then, the diluted particle solutions are nebulized until reaching the steady-state concentration, and the generation is stopped. Finally, the decay concentration measurements are continued utill reaching back to background concentration.

CHAPTER 3

RESULTS AND DISCUSSION

This chapter presents the numerical and experimental results and their discussion. The first section is devoted to ventilation experiments with the tracer gas method and the mean friction velocity obtained from the CFD simulation. The second section presents the experimental results related to the source characterization. Then, the numerical and experimental results are presented for the given scenario in chapter 2. Afterward, these results are compared and discussed from a different point of view.

3.1 Chamber ventilation

As presented in chapter 2, the verification of the well-mixed condition inside the chamber and the ventilation rate are determined experimentally via the tracer gas concentration decay method. The determined ventilation rates are imposed as the boundary conditions of CFD simulations to determine the mean friction velocity inside the chamber. The results are presented in the following subsections.

3.1.1 Ventilation rate and well-mixed condition verification

The measurements of tracer gas decay concentration are conducted in two different ventilation conditions. Each fan (inlet and outlet) is connected to a power supply. The flow rate delivered by the fans is adjusted by changing the supply voltage and current. For the first ventilation scenario, the power supply is adjusted to 4.0 V and 0.11 A and 6.0 V and 0.18 A for the second one. The CO_2 decay concentration is measured every second during the measurements. Then, the CO_2 concentration versus time measured by each device is plotted on a logarithmic scale. Finally, the regression of equation 2.6 is done for each measurement. The results for the three-measurement devices and both ventilation conditions are presented in Figures 3.1 and 3.2.

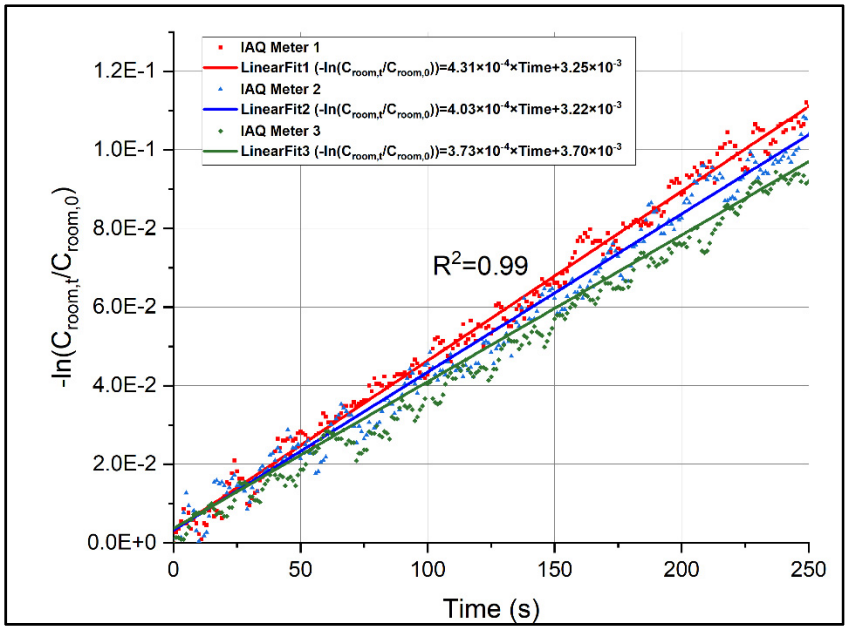

Figure 3.1 The logarithm decay concentration for the power supply condition of 4.0 V/0.11 A

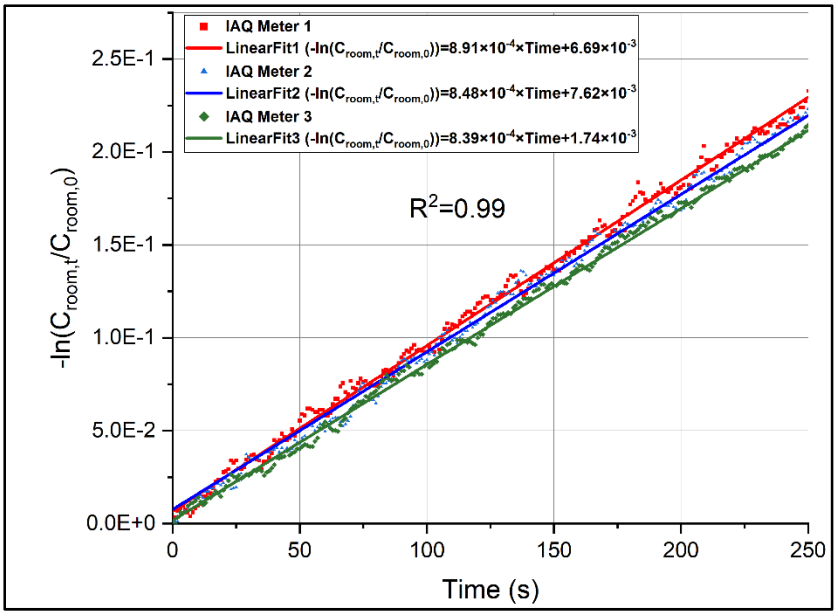

Figure 3.2 The logarithm decay concentration for the power supply condition of 6.0 V/0.18 A

Figures 3.1 and 3.2 presents the linear regression fits and the measured decay of the CO_2 concentration in the logarithm scale. The R-Squared of the regression for each measurement is 0.99, indicating a well-fit between the linear regression model and the data.

The curve's slope of presented linear fits in Figures 3.1 and 3.2 are representative of the term $\frac{Q}{V}$ in equation 2.6. For the linear regression fit of IAQ 1, IAQ 2, and IAQ 3, the slope of the curves in Figure 3.1 is equal to 4.13×10^{-4} s^{-1}, 4.03×10^{-4} s^{-1}, and 3.73×10^{-4} s^{-1} respectively. Since the chamber volume is 0.512 m^3, the airflow rates are equal to 2.12×10^{-4} m^3/s, 2.06×10^{-4} m^3/s, and 1.91×10^{-4} m^3/s, respectively, for the linear regression fit of IAQ 1, IAQ 2, and IAQ 3. These airflow rates give the ACH 1.49 hr^{-1}, 1.45 $hr^{-1,}$ and 1.34 hr^{-1}.

The slopes of curves in Figure 3.2 are equal with 8.91×10^{-4} s^{-1}, 8.48×10^{-4} s^{-1}, and 8.39×10^{-4} s^{-1} for the linear regression of IAQ 1, IAQ 2, and IAQ 3. The representative airflow rates of the linear regression of IAQ 1, IAQ 2, and IAQ 3 are 4.56×10^{-4} m^3/s, 4.34×10^{-1} m^3/s, and 4.30×10^{-4} m^3/s, respectively. The representative ACH of these flow rates are 3.21 hr^{-1}, 3.05 $hr^{-1,}$ and 3.02 hr^{-1}. The average values of measured airflow rates and the standard deviation are presented in Table 3.1.

Table 3.1 The average airflow rate of the chamber

Supply Fan voltage (V)	Supply Fan current (A)	Average Q and standard deviation (m^3/s)
4.0	0.11	$(2.05 \pm 0.10) \times10^{-4}$
6.0	0.18	$(4.40 \pm 0.14) \times10^{-4}$

The well-mixed condition is one of the main hypotheses of the WMR model, as noted in the methodology chapter. Thus, it is very important to verify whether the well-mixed condition is achieved or not. To verify this hypothesis, the average difference between the measured CO_2 concentrations is determined. The average difference between the measured CO_2 concentration are 9 ppm and 12 ppm, respectively, for the lowest and highest ACH. Since the average difference between the measured values is less than 50 ppm, it can be concluded that the well-

mixed condition as one of the central hypotheses of the model is achieved in both ventilation scenarios.

3.1.2 Mean friction velocity

As reviewed in Chapter 2, CFD simulation is employed to determine the friction velocity. The CFD computational domain includes the chamber and the mixing fan. The flow rates presented in Table 3.1 are imposed as boundary conditions at the inlet of the CFD model. The mixing fan is modelled as a ventilation duct with a length of 10 cm and a cross-section of 0.025 m^2. The air is drawn into this duct at one end and is blown at the other end. The velocity of blown air is 4.8 m/s. This velocity is measured experimentally by air velocity meter (velocicalc 7545). The air flow rate is set to 0.12 m^3/s, and the turbulence level is fixed at 10 %.

The CFD simulation is performed for 60 seconds. This simulation time is enough to achieve steady-state conditions and a stable time average value for the mean friction velocity from 24 points on the wall surfaces. Four points are located on each vertical surface of the chamber, 4 points on the floor of the chamber, and 4 points on the ceiling. The mean friction velocities with respect to time and for each ACH are presented in Figure 3.3.

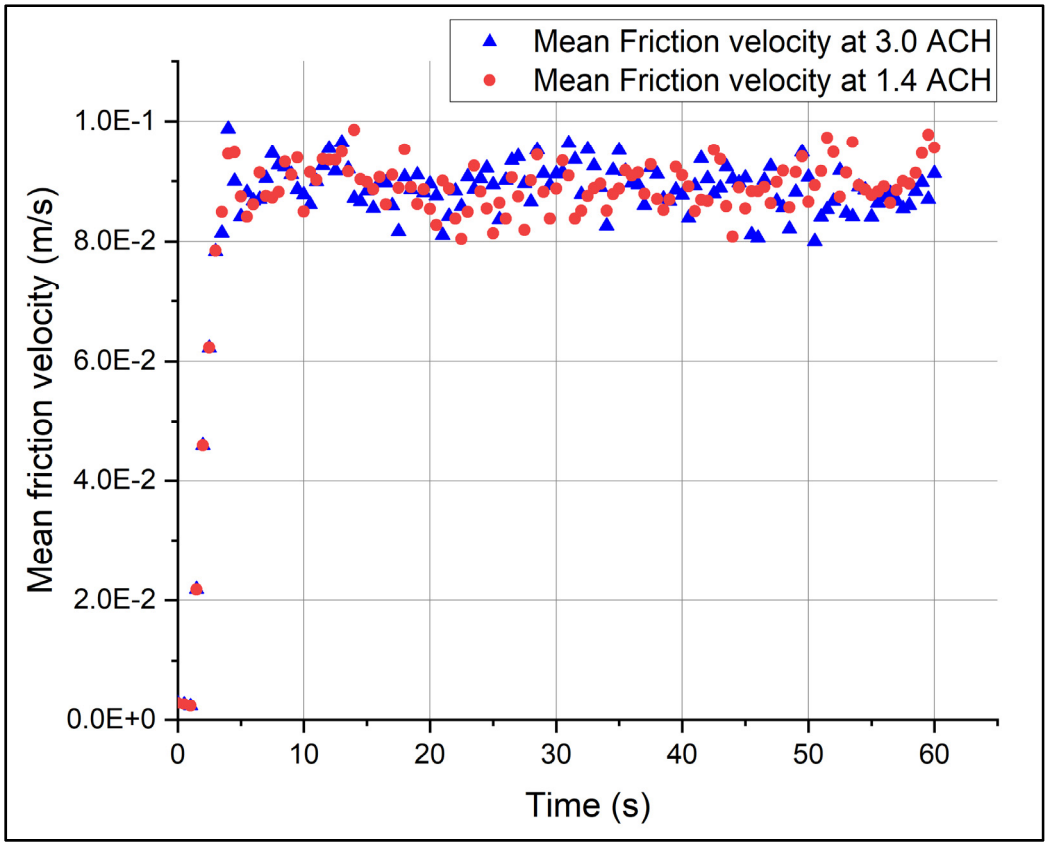

Figure 3.3 Mean friction velocity inside the chamber

The results indicate that the flow is well established after 20 seconds. Thus, the average of the mean friction velocity is calculated from 20 seconds to 60 seconds. The average mean friction velocity and their standard deviations for the lowest and highest ACH are as follows: $(8.87 \pm 0.36) \times 10^{-2}$ m/s and $(8.88 \pm 0.38) \times 10^{-2}$ m/s. These two values are very close to each other, and it can be related to the outflow's velocity of the inside mixing fan and ventilation fans.

The velocity at the inside mixing fan outlet is four times higher than the velocity at the ventilation fan. Therefore, the velocity field inside the chamber is mainly affected by the flow generated by the mixing fan, and the flow generated by the air inlet plays a minor role. Consequently, the mean friction velocity is similar in both ACHs. The mean average friction velocity obtained from CFD simulation results is used inside the WMR model to determine the deposition rate.

3.2 Source characterization

The mathematical term related to the generation rate from a source of contaminants (G) is present in all equations from 2.1 to 2.4. Thus, it is important to determine the closest value of the generation rate to the actual value by characterizing the generation source of contaminants. Moreover, the generation time to reach the steady-state condition should be investigated to have an insight into generation stopping time.

Firstly, particle size distributions are determined to estimate the generation rate. Secondly, the time to reach the steady-state condition is determined by generating the particles inside the chamber until reaching the steady-state concentration. These steps are explained in the following subsections.

3.2.1 Particle size distribution

The airborne particle size distribution for each particle dilution (1, 2, and 3 μm) is determined experimentally with the MetOne instrument. The measurements are based on the hypothesis that there are zero particles below and over the size range of the MetOne. Figures 3.4A to 3.4C present the size distribution of 1 μm, 2 μm, and 3 μm particle dilution.

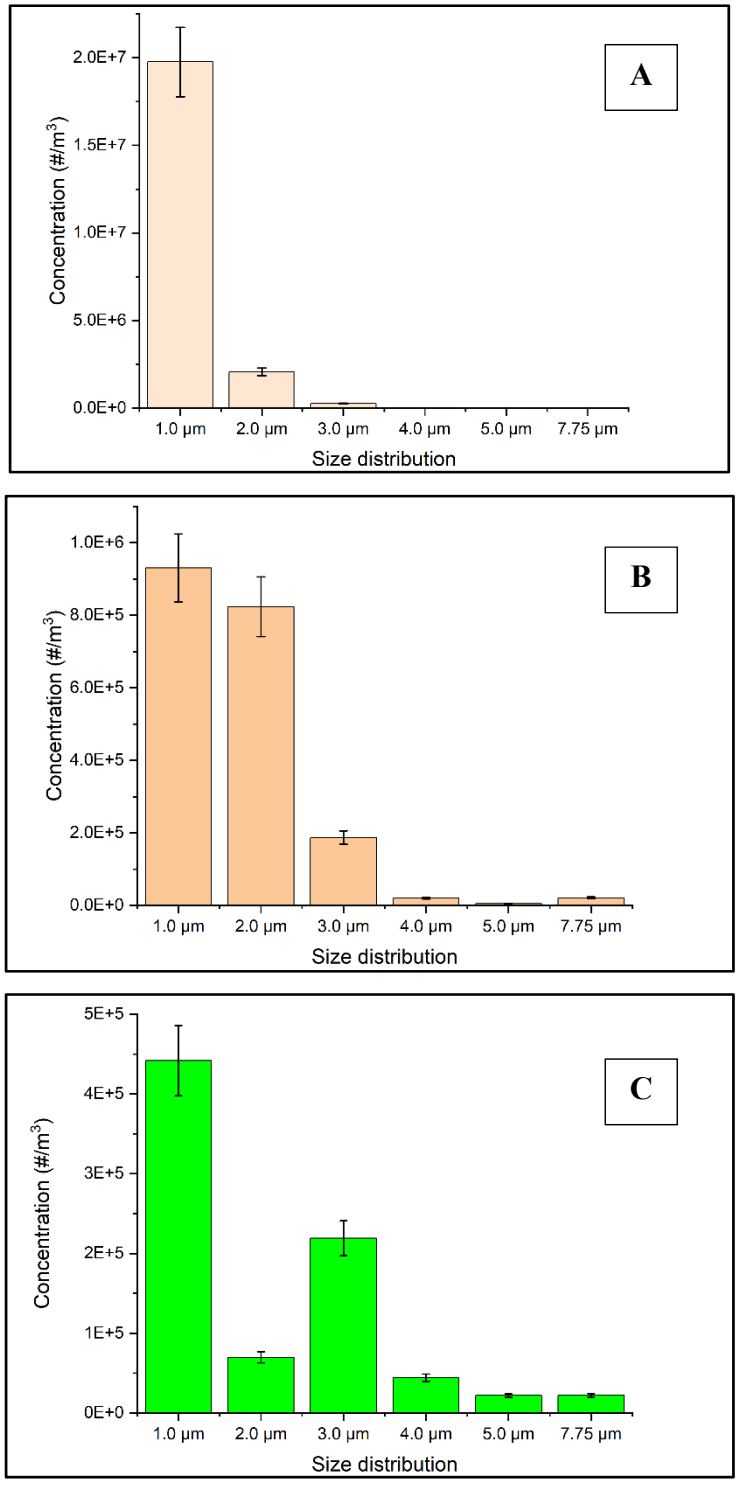

Figure 3.4 The particle size distribution for
the particle dilution of A)1 µm B) 2 µm and C) 3 µm

The presented error bars in Figure 3.4 are related to the device uncertainty through measuring the particle concentration measured by OPC. The results indicate that the generated aerosol from the nebulizer is not monodisperse except for 1 μm, and other particle sizes exist inside each dilution. The existence of different particle sizes can be related to two items. Firstly, particle coagulation can be occurred inside the dilution to form larger particle sizes. Secondly, the employed particles are an aqueous suspension. This may affect the particle size distribution over time due to hydrogen bonds or Van der Waals interactions.

As mentioned before, one of the objectives of source characterization is estimating the generation rate. The size distribution presented in Figure 3.4 is utilized to find the portion of mass loss attributed to specific particle size through the total mass loss of the dilution. This is done by determining the ratio of the mass of particles for a specific size to the total number of particles. This ratio multiplies by the mass loss of the dilution to determine the mass loss attributed to the related particle size. According to this method, the generation rates of experimental scenarios are determined, and the results are presented in Table 3.2.

Table 3.2 Particle generation rate

Scenarios	Generation rate (mg/min)	Particle Size (μm)
1	2.52×10^{-4}	1
2	1.59×10^{-4}	2
3	1.06×10^{-4}	3
4	3.29×10^{-4}	1
5	1.71×10^{-4}	2
6	1.11×10^{-4}	3

3.2.2 Steady-state condition

Each particle dilution is generated inside the chamber according to the scenarios presented in Table 2.2. The particle generation is continued until reaching a steady-state concentration. The findings are used to determine the time to reach the steady-state condition that applies to the main experiments.

The time to reach the steady-state condition determined by experiments can be compared with the time predicted numerically. Theoretically, reaching a steady-state concentration is impossible since the exponential time term in equation 2.4 never reaches zero. However, an estimation of the required time to reach the steady-state condition can be determined by an algebraic manipulation in equation 2.4. It can be solved by determining the required time to reach a concentration near the steady-state concentration, such as reaching 95% of steady-state concentration. By employing the mentioned algebraic manipulation, the time to reach the steady-state condition can be determined numerically. The time to reach the steady-state condition is determined numerically for each scenario and compared with experimental results. The results of the comparison are presented in Figure 3.5.

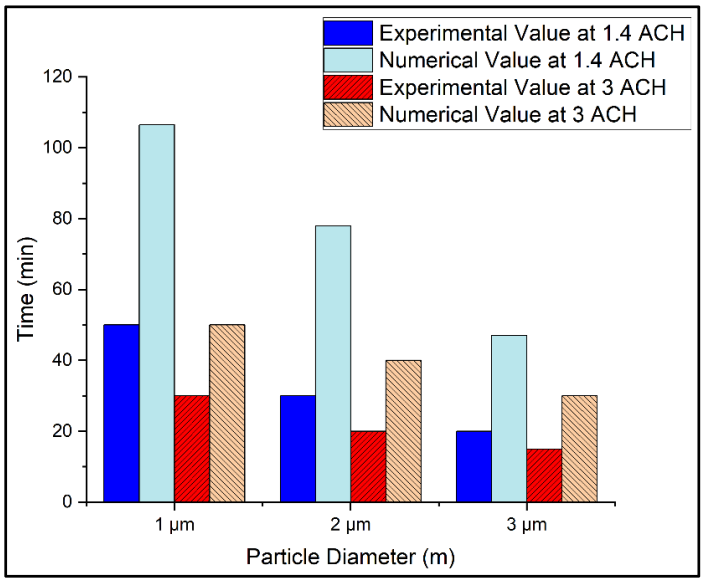

Figure 3.5 The comparison of time to reach the steady-state condition determined experimentally and numerically

These results indicate that the time to reach the steady-state condition varies for different particle sizes and ventilation rates. The experimental time to reach the steady-state value is determined at 1.4 ACH and equal with 50 minutes, 30 minutes, and 20 minutes for 1 µm, 2 µm, and 3 µm, respectively. For 3 ACH, it needs to generate the particle for 30 minutes, 20 minutes, and 15 minutes for 1 µm, 2 µm, and 3 µm, respectively, to reach the steady-state condition. The observed differences are related to the role of ventilation rates. According to equation 2.4, by increasing the term Q the time to reach the steady-state value decreases.

In Figure 3.5, the numerical results overestimate the experimental values. As an illustration, the time to reach the steady-state condition determined by the numerical results is 2.1 times higher than the experimental results for 1 µm particle at 1.4 ACH. Likewise, the predicted numerical value for 2 µm and 3µm are almost two times higher than the experimental value at 1.4 ACH. Lastly, the numerical values overestimate the experimental values 1.6 times for 1 µm and 2 times for 2 µm, and 3 µm at 3 ACH.

The observed overestimation can be related to the difference between the deposition rate estimated numerically and the actual value. The deposition rate of particles is one of the mathematical terms in equation 2.4 that can affect the time to reach the steady-state condition. The required time to reach the steady-state will increase as much as the deposition rate decrease. Therefore, the observed overestimation could be related to the numerical deposition rate. The next sections show that the numerical deposition rate underestimates the actual value.

3.3 Numerical and experimental results

As explained in the methodology chapter, three deposition velocities are considered to predict the deposition rate of aerosols inside the chamber. Then, six experimental tests are performed to cross over different sizes of particles (1 µm, 2 µm, and 3 µm) and 2 ACH (1.4 hr^{-1} and 3.0 hr^{-1}), and experimental results are compared with the numerical results. In the following,

the predicted deposition rate is presented firstly. Then, the comparison of experimental and numerical results and their discussion are given.

3.3.1 Deposition rates

The deposition rate of 1 µm, 2 µm, and 3 µm particles are predicted by the mathematical relationship of Wood 1981, Charurau 1982, and Lai, and Nazaroff 2002. The average of presented friction velocity in section 3.1.2 is employed for determining the deposition rates. The results of predicted depositions are presented in Figure 3.6.

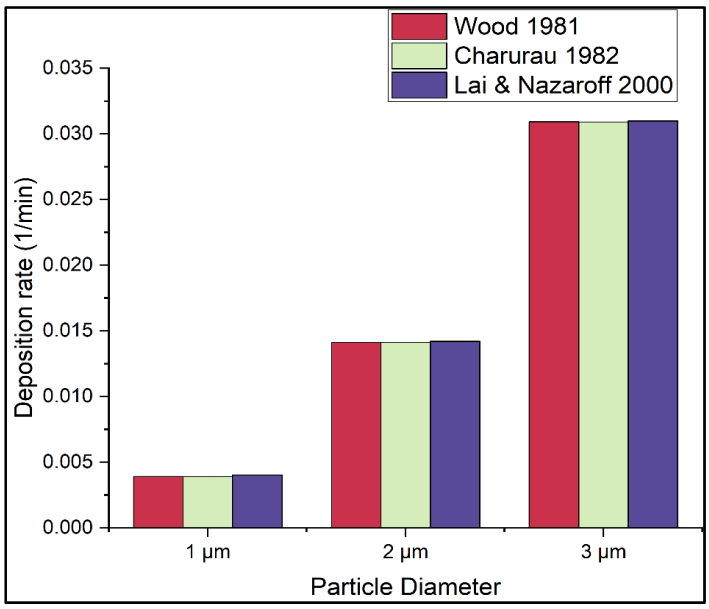

Figure 3.6 Predicted deposition rates
of 1 µm, 2 µm, and 3 µm particles

The predicted deposition rates by Woods, Charurau and Lai and Nazaroff for 1 µm particle are 3.92×10^{-3} min^{-1}, 3.90×10^{-3} min^{-1} and 4.03×10^{-3} min^{-1} respectively. Woods, Charurau, and Lai, and Nazaroff anticipate the deposition rates for 2 µm particles as follows: 1.41×10^{-2} min^{-1}, 1.41×10^{-2} min^{-1}, and 1.42×10^{-2} min^{-1}. For the 3 µm particles, the predicted deposition rates by Woods, Charurau and Lai and Nazaroff are 3.09×10^{-2} min^{-1}, 3.09×10^{-2} min^{-1}, and 3.10×10^{-2} min^{-1}.

The results indicate that the particle deposition rate rises by increasing the diameter of the particles. This increase can be explained as follows. The mass of the particles increases by growing up the diameter of particles. The increase of the mass leads to intensifying the effects of gravity on particle deposition. Thus, the larger particles have a higher deposition rate, as can be seen in Figure 3.6.

As shown in Figure 3.6, the average difference between the predicted deposition rate models is less than 2%, and the values of the predicted deposition rates are close to each other. Therefore, only one numerical curve is considered for these three deposition models in the following sections.

3.3.2 Scenarios' results

Six experimental scenarios are performed and compared with the numerical results. The results of each experiment and its comparison with the numerical result are presented in Figures 3.7 and 3.8.

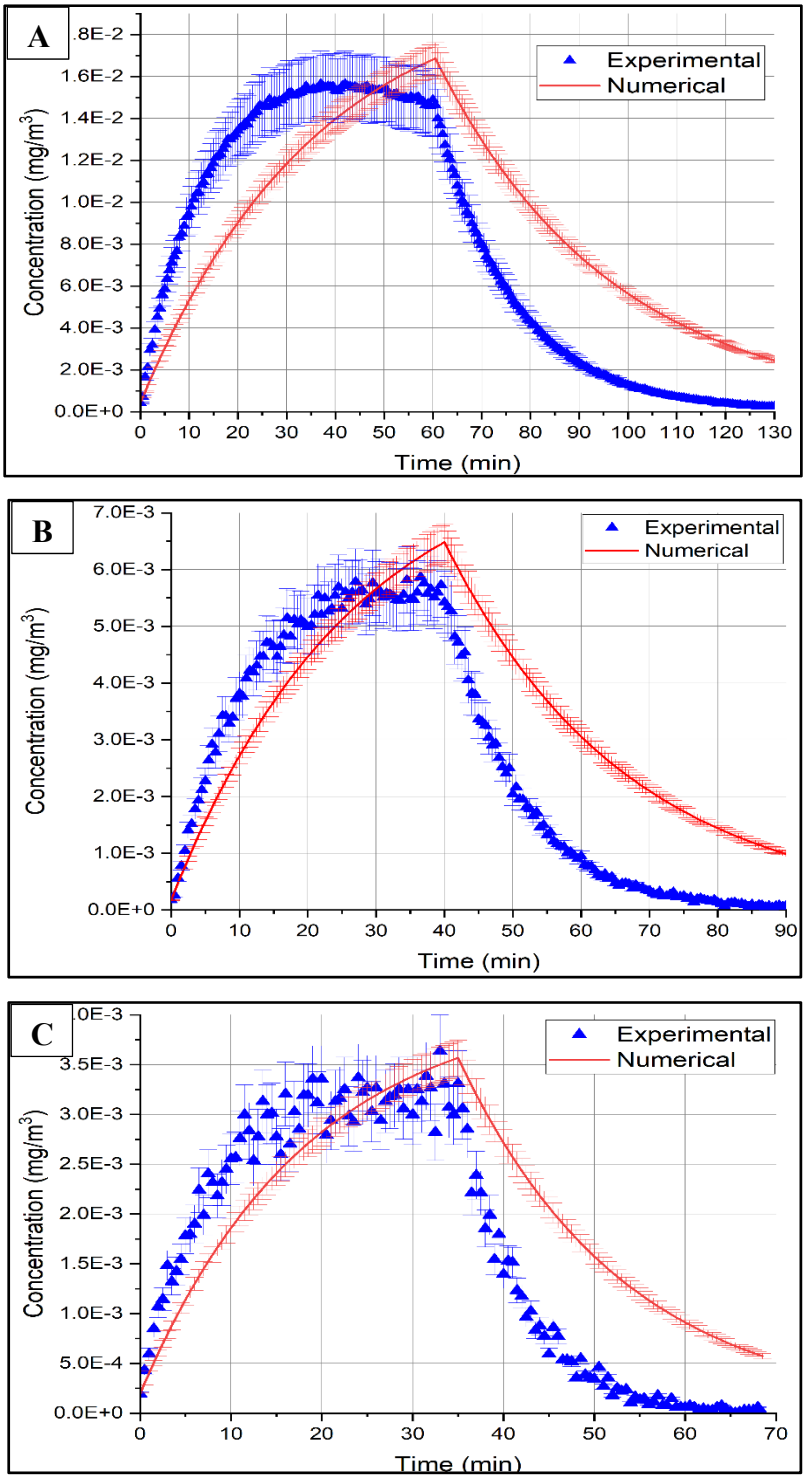

Figure 3.7 The comparison of numerical and experimental results for 1.4 ACH: A) 1 µm B) 2 µm C) 3 µm

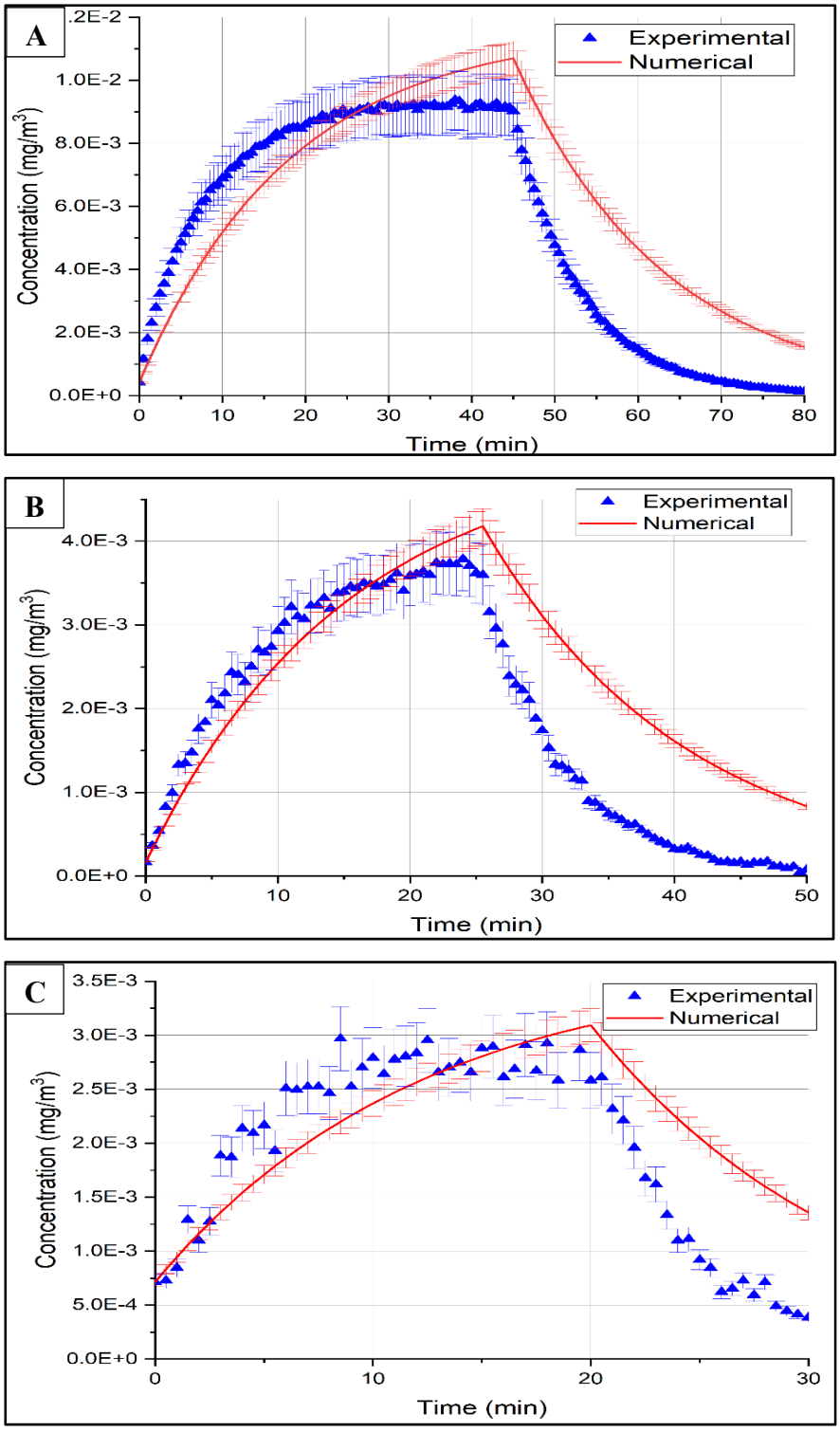

Figure 3.8 The comparison of numerical and experimental results for 3.0 ACH: A) 1 µm B) 2 µm C) 3 µm

The experimental and numerical results are displayed with their error bars. The error bars in the experimental results are caused by the measurement uncertainty of the OPS. The error bars in the numerical results are related to the uncertainties associated with the generation rate and the ACH. The presented results in Figure 3.7 and Figure 3.8 are discussed in the following paragraphs.

The results show that the particle dispersion in the experimental results for different particle sizes is not identical. The blue triangles scattered very close to each other for 1 μm, which is not the same for 2 μm and 3 μm. The main reason is related to the concentration of particles inside the employed dilution. The 1 μm dilution is 8 times more concentrated than the 2 μm dilution and 27 times 3 μm. As observed a higher concentration leads to lower dispersion.

The curves in Figures 3.7 and 3.8 can be discussed in two parts, generation period and decay period. In the generation period, the numerical and experimental results agree by considering their error bar. However, the numerical and experimental results diverge during the decay period.

During the decay period, the numerical results overestimate the real concentration value. In Figure 3.7a, the numerical and experimental curves diverge from each other from minute 65 to the end of the experiment. This trend is observed in Figures 3.7b and 3.7c that the numerical and experimental curves started to deviate from each other at minutes 45 and 35 to the end of the experiment.

In Figure 3.8, the numerical results overestimate the concentration determined experimentally during the decay period, as observed in Figure 3.7. In Figure 3.8a, the numerical decay concentration overestimates the real value and starts to diverge from the experimental result at minute 45 to the end of the experiments. Figures 3.8b and 3.8c show that the numerical decay concentration deviated from the experimental decay curve at minutes 45 and 20 until the last minutes, respectively.

The observed overestimation can be related to the removal mechanisms that are not considered inside the model. As noted in chapter 2, the numerical model is only considering the gravitational settling and Brownian and turbulent deposition. However, there are other mechanisms exist that can lead to the removal of particles. One of the mechanisms that is not considered inside the model is particle coagulation. According to the size distribution results presented in Figure 3.4, other particle sizes exist with different sizes and concentrations in each dilution. The existence of these particles increases the chance of particle-particle collisions and cause particle coagulation occurs (Rim *et al.*, 2012). Since the coagulation of the particles affects the number of particles, it can be concluded that neglecting the coagulation mechanism in the numerical model leads to overestimating the particle's decay concentration. The effects of other neglected mechanisms are explained in the following sections.

3.3.3 The effects of deposition

The deposition rate is one of the terms that affect the concentration decay, as presented in the methodology chapter. According to equation 2.4, the underestimation of deposition rate in the numerical model leads to overestimating the concentration decay. The deposition rate employed in the model only considers the gravitational settling and the Brownian and turbulent diffusion and neglect other mechanisms. There could be other potential deposition mechanisms that affect the deposition rate in real environments.

The particles supplier (Polysciences) announced that the provided particles have an anionic charge from sulfate ester. Moreover, there is a high chance of electrostatic charges accumulation on the surface of the chamber and nebulizer, which is not considered. The surfaces of the chamber were contacted during the cleaning and installation. Moreover, during the filling of the nebulizer, the jar and other components were touched by hand. The mentioned reasons lead to having a potential electrostatic charge that can cause electrostatic depositions. The electrostatic deposition is not included in the numerical model. It leads to underestimating the real deposition rate.

To show the effects of the deposition rate in the decay period, the concentration predicted by the WMR model is determined for five deposition coefficients. The first scenario uses the deposition rate as same as the Lai and Nazaroff correlation result (β=0.004 min^{-1}). The other four scenarios employ the following deposition rates: β_1=0.01 min^{-1}, β_2=0.02 min^{-1}, β_3=0.03 min^{-1}, and β_4=0.04 min^{-1}. The results of these scenarios are compared with the experimental result in the decay period for 1 μm at 1.4 ACH. The results are presented in Figure 3.9.

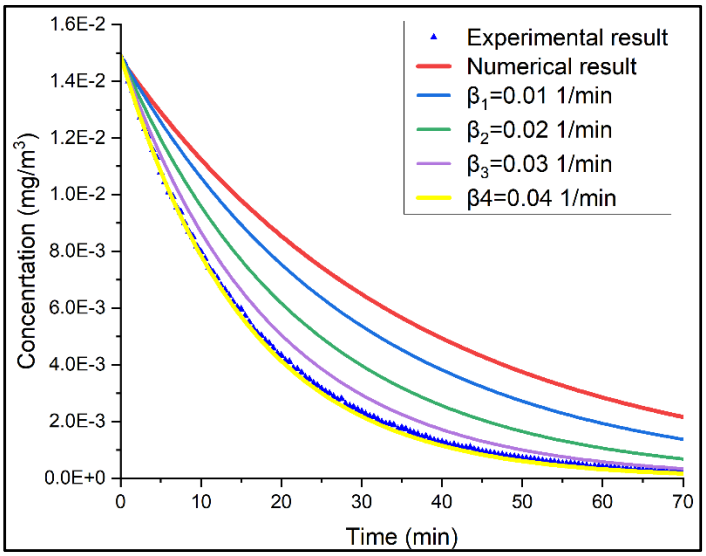

Figure 3.9 The comparison of different deposition rates and experimental value

As can be seen, the decay concentration is highly affected by the deposition rate. By increasing the deposition rate, the numerical decay concentration moves toward the experimental results. It can prove that underestimating the deposition rate leads to overestimating the decay concentration.

Consequently, particle deposition is significant, and it is important to consider not only the gravitational settling and the Brownian and turbulent deposition but also other removal mechanisms such as electrostatic deposition.

3.3.4 Input parameter uncertainty

The other point that should be discussed is the dependency of the numerical results on the uncertainty of input parameters. Previous studies that employed the WMR model concluded that the model is highly dependent on the input parameters. A small uncertainty of the input parameters can greatly affect the numerical results (Hewett et Ganser, 2017 ; Mølgaard *et al.*, 2014). To verify the effects of the input parameters on the model results, three scenarios are designed. The scenarios are presented in Table 3.3.

Table 3.3 Scenarios for verifying the effects of input parameters

Scenarios	Fixed Parameters	Vary Parameters
1	Q_2=0.012 m^3/min, G_2=2.52E-04 mg/min	β_1=0.0135 min^{-1} **β_2=0.0150 min^{-1}** β_3=0.0165 min^{-1}
2	β_2= 0.015 min^{-1}, G_2=2.52E-04 mg/min	Q_1=0.0108 m^3/min, **Q_2=0.0120 m^3/min,** Q_3=0.0132 m^3/min,
3	Q_2=0.012 m^3/min, β_2= 0.015 min^{-1}	G_1=2.27E-04 mg/min, **G_2=2.52E-04 mg/min,** G_3=2.77E-04 mg/min,

Each scenario includes a base case (case 2; in bold), and two other cases are included a 10% decrease (case 1) or increase (case 3) on the input parameters. The results of these scenarios are presented in Figure 3.10.

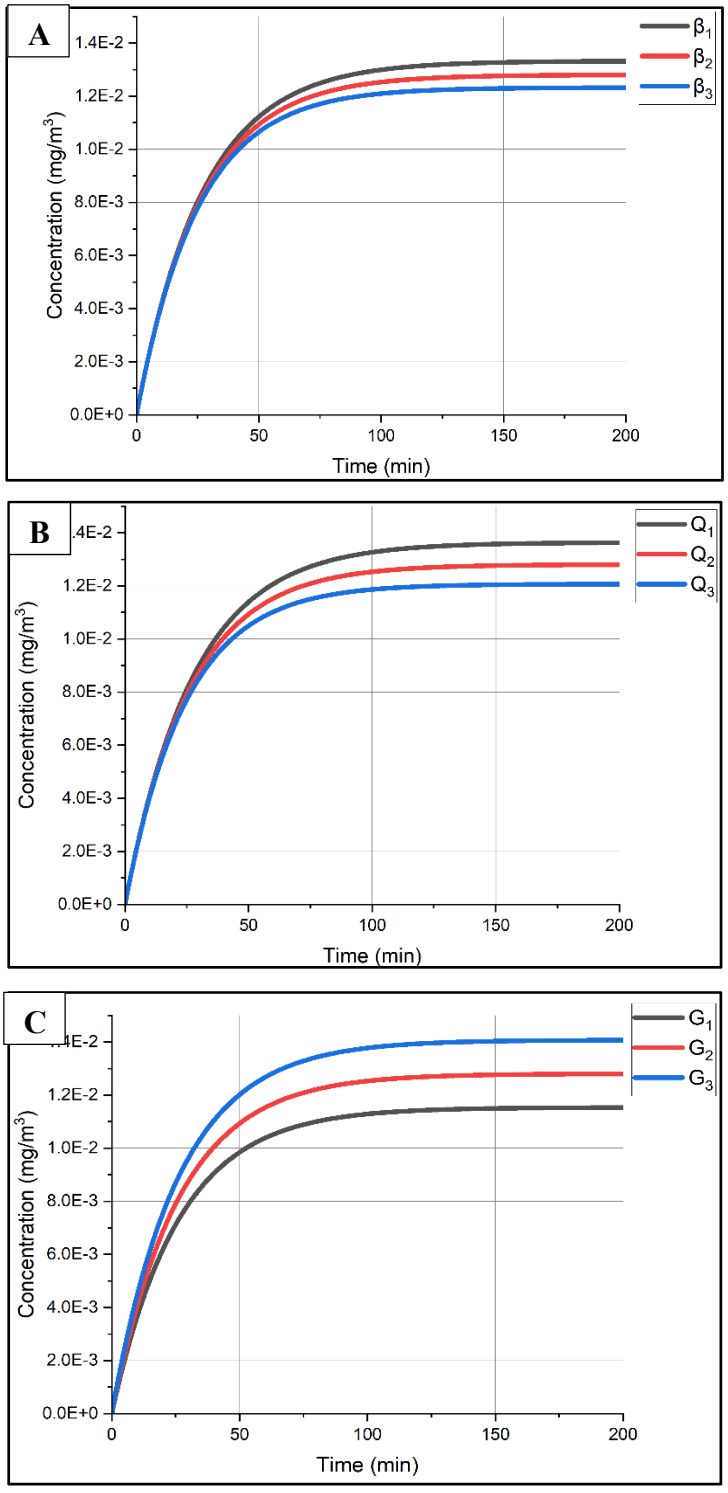

Figure 3.10 The effects of changing input parameters: A) changing β, B) changing Q and C) changing G

The steady-state value of the concentrations differs 3.9 % by changing deposition rate, 5.7 % by changing ventilation rate, and 9.0% by changing the generation rate. Among the parameters, the deposition rate variation has less effect on the results than the airflow rate and generation rate, as shown in Figure 3.10. The highest effect is related to changing the generation rate value. Many previous studies stated that estimating the generation source is one of the main challenges, and a small difference in the value of the estimated generation rate can highly affect the predicted results by the model (Ribalta, Koivisto, López-Lilao, *et al.*, 2019), which is also observed in the Figure 3.10.

3.3.5 Stability of solutions in the nebulizer

According to the finding of the previous section, the generation rate highly affects the numerical result. Thus, extra experiments were performed on the generation source.

Two experimental scenarios are chosen to check the stability of the solution in the nebulizer. In the first scenario, the nebulizer is filled with a "fresh dilution" and generates the particles until reaching the steady-state condition. Fresh dilution refers to the dilution that is prepared just before the experiment and never used inside the jar of the nebulizer. In the second scenario, the nebulizer is filled with "used dilution" and generates the particles to reach the steady-state concentration. The old dilution refers to a dilution that is used once inside the jar of nebulizer for 60 minutes of generation.

During the experiments, the particle concentration is measured by MetOne OPS. The results of these analyses can be helpful to have an insight into changing the concentration of dilution over time. The temporal evolution of the particle number concentrations per m^3 measured in the chamber for the used and fresh dilution of 1 μm and 2 μm and 3 μm particle is presented in Figure 3.11.

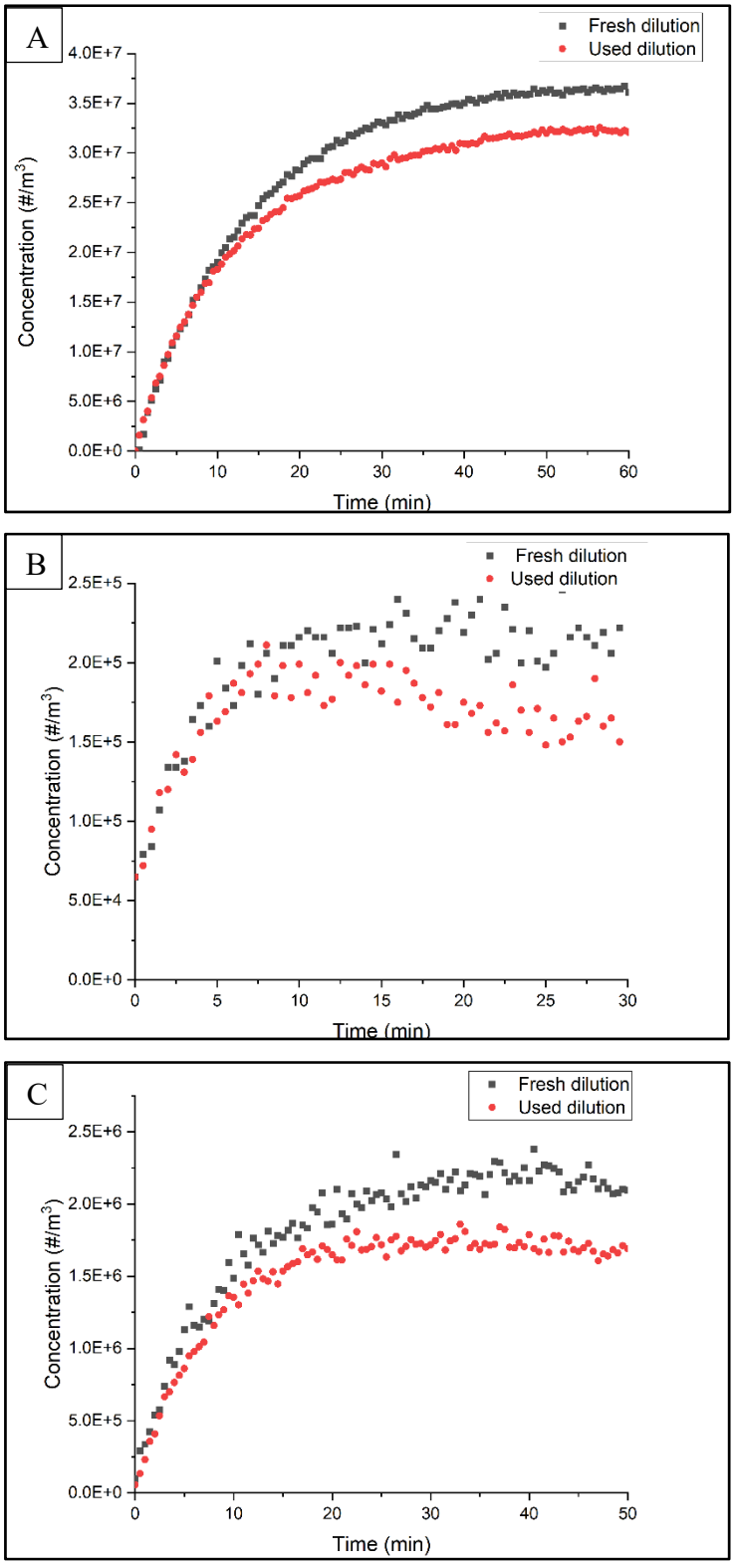

Figure 3.11 Particle concentration of fresh and used dilution for:
A) 1 µm, B) 2 µm and C) 3 µm

The presented curves in Figures 3.11a to 3.11c are respectively for the channel at 1 μm, 2 μm, and 3 μm. The results indicate a difference between the concentration of fresh and used dilution. The observing differences between both dilutions can be related to the operation mechanisms of the nebulizer and the occurring chemical changes inside the dilutions over time.

The nebulizer employs a high-speed jet of compressed air through a small orifice that makes a negative pressure and siphons the liquid into the jet stream. The jets blow the liquid into the jar's wall of the nebulizer, and liquid droplets are generated. The large generated droplets (d_p > 5μm), deposited by inertial impaction and slip into the jar (Feng *et al.*, 2021). To put it simply, a small fraction of the liquid escapes the nebulizer, and more than 90% of the liquid goes back to the jar (Feng *et al.*, 2021 ; May, 1973). The returning liquid affects the concentration of dilution inside and causes the differences between the fresh and old dilution. It means that the concentration of dilution inside the jar of the nebulizer changes over time.

All the reasons mentioned in the above subsections cause differences between experimental and numerical results. In the model of this study, different deposition models are considered to improve the accuracy of the prediction value. However, the considered deposition models present almost identical deposition coefficients, and further investigations are required to improve the WMR model's accuracy.

CONCLUSION

The standard WMR model has been widely used to predict the concentration of gaseous contaminants in indoor environments. The main objective of this master's thesis was to determine experimentally whether the deposition of airborne particles is significant inside a small chamber.

To reach the objective of the project, numerical and experimental phases were done. The standard WMR model was modified with a term added to the mass conservation law to consider the gravitational settling and Brownian and turbulent deposition. These two mechanisms were chosen since they can significantly change the airborne concentration of aerosols and cause surface contamination. The deposition rate was predicted by three models: Wood 1981, Charurau 1982, and Lai and Nazaroff 2000. The analytic solution of the mass conservation law was coded to predict the contaminant concentration as a function of time inside the chamber.

In the experimental part, six experiments were performed inside a parallelepiped Plexiglas chamber equipped with mechanical ventilation. The chamber ventilation and verification of the well-mixed condition were measured by the tracer gas decay method. The results of tracer gas decay concentration indicate that the ACH of the chamber is equal to 1.4 and 3.0. Particles of 1, 2, and 3 μm in diameter were generated inside the chamber via a nebulizer until reaching the steady-state concentration. The concentration of particles was measured by an OPS. The experiments were designed to evaluate the mathematical model in various conditions that are representative of the real-world environment. The experimental scenarios included three-particle sizes and two ventilation rates (1.4 ACH and 3.0 ACH).

The numerical results showed that the average difference between the predicted deposition rate by the three models was less than 2%. The comparison between the numerical model and the experimental results shows a good agreement during the generation period. However, the modified WMR model overestimate significantly the experimental results in the decay period. This overestimation can be attributed to neglecting other removal mechanisms such as coagulation and other deposition mechanisms like electrostatic deposition and thermophoresis. Therefore, the considered deposition models were not sufficient to predict the particles concentrations and the deposition rates. Consequently, it is important to consider not only the gravitational settling and the Brownian and turbulent deposition but also electrostatic deposition.

LIMITATIONS AND RECOMMENDATIONS

The limitation of this study can be separated into model limitations and device limitations. The WMR model is limited to a well-mixed environment, which is not easily achieved in many indoors (Ribalta, Koivisto, Salmatonidis, *et al.*, 2019). Moreover, the considered removal mechanisms of particles inside the model are limited to ventilation and particle gravitational settling and the Brownian and turbulent diffusion. The model does not take into account the other removal mechanisms such as electrostatic deposition, thermophoresis, and coagulation.

The OPS and the nebulizer used in this study have the advantage that they are very cost-efficient compared with other devices in the market. However, they have some drawbacks. The particle counter is limited to the size range of 0.3 μm to 10 μm and does not measure the nanoscale particles. The nebulizer is limited to generating particles with a maximum diameter of 3 μm also maximum air is limited according to the material of the jar. These two limits narrow the domain of the experiment and limit further investigation with other sizes of particles.

For future studies, some recommendations can be considered. Firstly, it is recommended to consider other deposition mechanisms and coagulation to improve the model prediction accuracy. Furthermore, it is highly recommended to use the particle counter with wider size measurement, such as an aerodynamic particle sizer, to expand the domain of investigation. Using aerosol generators such as TSI 3482 monodisperse generators is suggested since it can generate other particle sizes. Also, a particle neutralizer is recommended to employ to reduce the chance of electro charges on particles. Moreover, it is suggested to use the dry particle to prevent the dilution stability challenges mentioned in chapter 3. Finally, it will be helpful to evaluate the model in real-world scenarios with a wider range of particle sizes to find out the limitation and strengths of the prediction model.

ANNEX I

CFD GOVERNING EQUATIONS

FDS software solves Navier-Stokes equations for low-velocity fluid with a MACH number less than 0.3 (McGrattan *et al.*, 2021). The code includes hydrodynamic modules, a combustion module, and a radiation module with participating media. In the context of this study, only the hydrodynamic module is used. The equations solved in this module are the following conservation equations:

Contaminant transport equation

$$\frac{\partial(\rho Z)}{\partial(t)} + \nabla\big(\rho Z(U)\big) = \nabla \cdot (\rho D \nabla Z) \tag{A I-1}$$

Perfect gas equation

$$H = \rho T R \sum \frac{Y_a}{M_a} \tag{A I-2}$$

Mass conservation

$$\frac{\partial \rho}{\partial t} + \mathrm{div}\big(\rho \vec{U}\big) = 0 \tag{A I-3}$$

Momentum conservation

$$\frac{\partial \rho U_i}{\partial t} + \frac{\partial\big(\rho u_i u_j\big)}{\partial x_j} = -\frac{\partial \rho}{\partial x_i} - \frac{\partial \tau_{ij}}{\partial x_i} + \rho g_i + f_{d,i} \tag{A I-4}$$

where the shear tensor is

$$\tau_{ij} = \mu(S_{ij} - \frac{2}{3}\delta_{ij}(\nabla \cdot \vec{u})) \tag{A I-5}$$

and the stress tensor is

$$S_{ij} = \frac{1}{2}(\frac{\partial u_i}{\partial x_j} + \frac{\partial u_j}{\partial x_i}) \tag{A I-6}$$

The mean friction velocity that is determined by the CFD results is calculated by:

$$\overline{u^*} = \frac{\sum_{i=1}^{n} u_i^* \times A_i}{\sum_{i=1}^{n} A_i} \quad \text{(A I-7)}$$

Where the index refers to the number of surfaces and u^* is the friction velocity (m/s), and A is the surface area of each surface (m^2). The mean friction velocity obtained from the CFD results includes 24 friction velocity values on surfaces as follows: 4 points at vertical surfaces of the chamber, 4 points on the floor of the chamber, and 4 points on the ceiling of the chamber. The schematic view of the grided chamber for the simulation is presented in Figure A I-1.

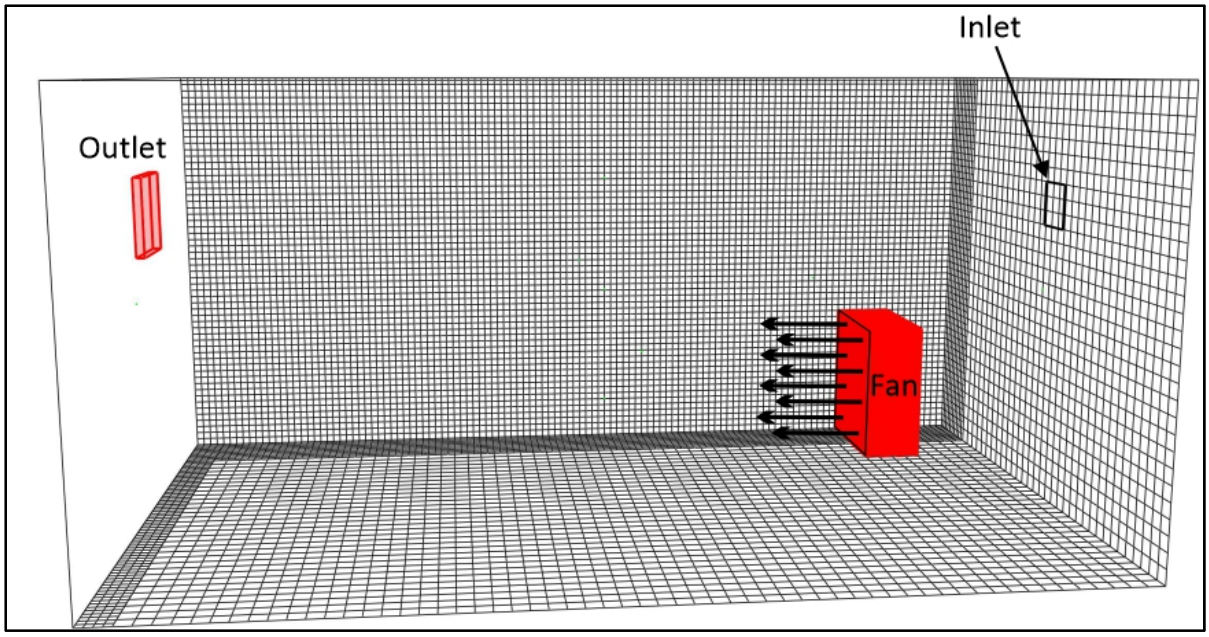

Figure-A I-3 The schematic layout of the grided chamber for the simulation

The Grid convergence index (GCI) is defined as:

$$GCI_{21} = \frac{1.25\varepsilon_{12}}{r_{21}^{p} - 1} \quad \text{(A I-8)}$$

Where r is the mesh ratio: $r_{21} = \frac{h_2}{h_1}$ $where\ h_1 < h_2$ and $h = \sqrt[3]{\frac{1}{N}\sum_{i=1}^{N} \Delta V_i}$. The power of r in the equation is equal to two (p=2) since FDS uses a 2nd order finite difference discretization scheme. Two meshes are considered for GCI. The details of each mesh are presented in Table A I-1. The difference between average friction velocity from mesh 1 and 2 is:

$\varepsilon_{12} = \left|u^*_{fric,1} - u^*_{fric,2}\right|$

Table-A I-1 The meshing details for the GCI

Parameters	Mesh 1	Mesh 2
Number of nodes (N)	140 418	66 120
h (m)	0.0156	0.020
v_{fric} (m/s)	0.241	0.252

The GCI_{21} is 0.85 % which is considered satisfactory and satisfies the need for determining the friction velocity.

ANNEX II

The comparison of optical particle counters

The GT-526S was compared with a well-known OPS TSI 3330 device and tested at Institut de recherche Robert-Sauvé en santé et en sécurité du travail (IRSST). The polystyrene particles are employed for the tests. The result of comparing is presented in Figure A II-1.

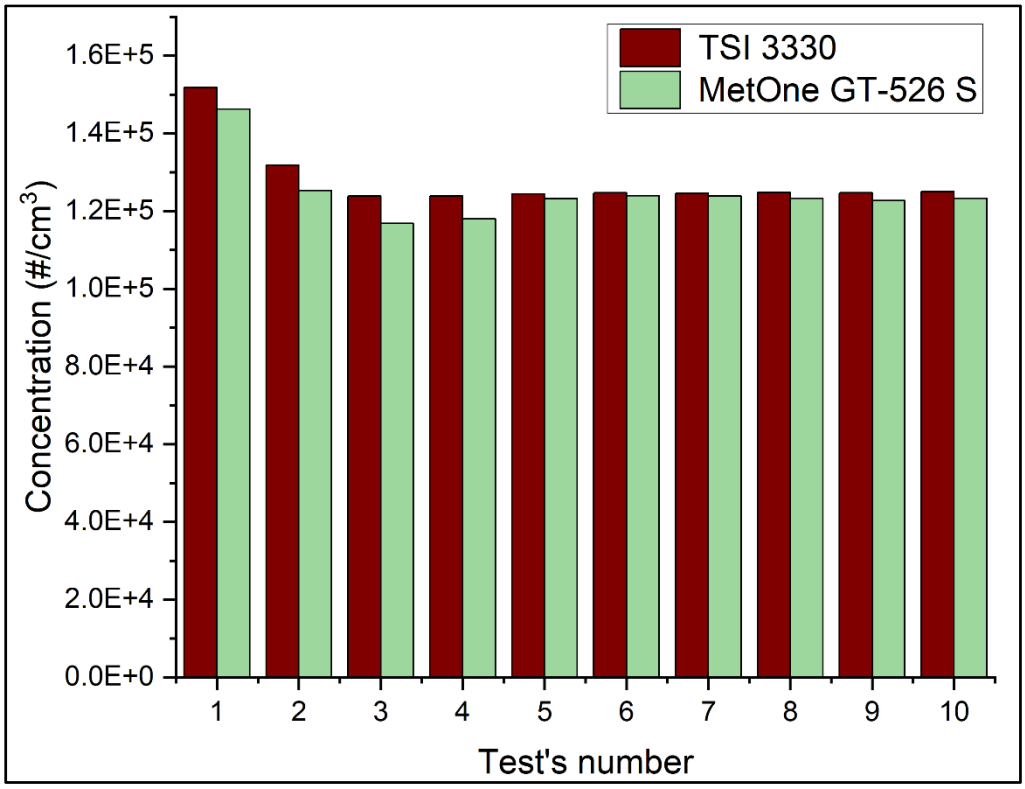

Figure-A II-1 The comparison of the two OPS': TSI 3330 and GT-526s

The comparison results indicate that the average difference between the value predicted by TSI 3330 and GT-526S is less than 3%. Therefore, MetOne can be used as a low-cost device in measuring particle concentration.

LIST OF BIBLIOGRAPHICAL REFERENCES

Agarwal, Tarun K., B. K. Sahoo, Mukesh Kumar et B. K. Sapra. 2021. « A Computational Fluid Dynamics code for aerosol and decay-product studies in indoor environments ». *Journal of Radioanalytical and Nuclear Chemistry*. <https://doi.org/10.1007/s10967-021-07877-8>.

Arnold, Susan F., Yuan Shao et Gurumurthy Ramachandran. 2017. « Evaluating well-mixed room and near-field–far-field model performance under highly controlled conditions ». *Journal of Occupational and Environmental Hygiene*, vol. 14, nº 6, p. 427-437. <https://doi.org/10.1080/15459624.2017.1285492>.

Arnold, Susan, Gurumurthy Ramachandran, Hannah Kaup et Joseph Servadio. 2020. « Estimating the time-varying generation rate of acetic acid from an all-purpose floor cleaner ». *Journal of Exposure Science & Environmental Epidemiology*, vol. 30, nº 2, p. 374-382. <https://doi.org/10.1038/s41370-019-0142-5>.

ASTM Committee D22. 2019. *Guide for Statistical Evaluation of Indoor Air Quality Models*. ASTM International. <https://doi.org/10.1520/D5157-19>.

Avino, Pasquale, Maurizio Manigrasso, Pietro Pandolfi, Cosimo Tornese, Diego Settimi et Nicola Paolucci. 2015. « Submicron particles during macro-and micro-weldings procedures in industrial indoor environments and health implications for welding operators ». *Metals*, vol. 5, nº 2, p. 1045-1060.

Bierkandt, Frank S., Lars Leibrock, Sandra Wagener, Peter Laux et Andreas Luch. 2018. « The impact of nanomaterial characteristics on inhalation toxicity ». *Toxicology Research*, vol. 7, nº 3, p. 321-346. <https://doi.org/10.1039/c7tx00242d>.

Blocken, Bert, Ted Stathopoulos, Jan Carmeliet et Jan Hensen. 2009. « APPLICATION OF CFD IN BUILDING PERFORMANCE SIMULATION FOR THE OUTDOOR ENVIRONMENT ». p. 8.

Buonanno, Giorgio, Lidia Morawska et Luca Stabile. 2011. « Exposure to welding particles in automotive plants ». *Journal of Aerosol Science*, vol. 42, nº 5, p. 295-304.

Butt, Edward W., Steven T. Turnock, Richard Rigby, Carly L. Reddington, Masaru Yoshioka, Jill S. Johnson, Leighton A. Regayre, Kirsty J. Pringle, Graham W. Mann et Dominick V. Spracklen. 2017. « Global and regional trends in particulate air quality and attributable health burden over the past 50 years ». In *EGU General Assembly Conference Abstracts*. (2017), p. 3519.

Cao, Qing, Chun Chen, Sumei Liu, Chao-Hsin Lin, Daniel Wei et Qingyan Chen. 2018. « Prediction of particle deposition around the cabin air supply nozzles of commercial airplanes using measured in-cabin particle emission rates ». *Indoor air*, vol. 28, nº 6, p. 852-865.

Changfu, You et Li Guanghui. 2008. « Direct Numerical Simulation of Microparticle Motion in Channel Flow with Thermophoresis ». *Journal of Environmental Engineering*, vol. 134, nº 2, p. 138-144. <https://doi.org/10.1061/(ASCE)0733-9372(2008)134:2(138)>.

Cooper, Douglas W., Michael H. Peters et Robert J. Miller. 1989. « Predicted Deposition of Submicrometer Particles Due to Diffusion and Electrostatics in Viscous Axisymmetric Stagnation-Point Flow ». *Aerosol Science and Technology*, vol. 11, nº 2, p. 133-143. <https://doi.org/10.1080/02786828908959306>.

Csavina, Janae, Jason Field, Mark P. Taylor, Song Gao, Andrea Landázuri, Eric A. Betterton et A. Eduardo Sáez. 2012. « A review on the importance of metals and metalloids in atmospheric dust and aerosol from mining operations ». *Science of The Total Environment*, vol. 433, p. 58-73. <https://doi.org/10.1016/j.scitotenv.2012.06.013>.

Dols, W Stuart, Andrew K Persily et Brian J Polidoro. 2018. *Development of CPSC nano-particle modelling tools*. NIST TN 2004. Gaithersburg, MD : National Institute of Standards and Technology, NIST TN 2004 p. <https://doi.org/10.6028/NIST.TN.2004>.

Esteban Florez, Fernando Luis, Tyler Thibodeau, Toluwanimi Oni, Evan Floyd, Sharukh S. Khajotia et Changjie Cai. 2021. « Size-resolved spatial distribution analysis of aerosols with or without the utilization of a novel aerosol containment device in dental settings ». *Physics of Fluids*, vol. 33, nº 8, p. 085102. <https://doi.org/10.1063/5.0056229>.

Fan, Fa-Gung et Goodarz Ahmadi. 1994. « On the Sublayer Model for Turbulent Deposition of Aerosol Particles in the Presence of Gravity and Electric Fields ». *Aerosol Science and Technology*, vol. 21, nº 1, p. 49-71. <https://doi.org/10.1080/02786829408959696>.

Feng, James Q., Liang-Sin Go, Jenny Calubayan et Robert Tomaska. 2021. « Working Mechanism and Behavior of Collison Nebulizer ». *Aerosol Science and Engineering*, vol. 5, nº 3, p. 285-291. <https://doi.org/10.1007/s41810-021-00102-9>.

Ha, Tae Woong et Bok Seong Choe. 2014. « Numerical prediction of rotordynamic coefficients for an annular-type plain-gas seal using 3D CFD analysis ». *Journal of Mechanical Science and Technology*, vol. 28, nº 2, p. 505-511. <https://doi.org/10.1007/s12206-011-0830-3>.

Hartmann, G. C., L. M. Marks et C. C. Yang. 1976. « Physical models for photoactive pigment electrophotography ». *Journal of Applied Physics*, vol. 47, nº 12, p. 5409-5420. <https://doi.org/10.1063/1.322571>.

Hefny, Mohamed M. et Ryozo Ooka. 2009. « CFD analysis of pollutant dispersion around buildings: Effect of cell geometry ». *Building and Environment*, vol. 44, nº 8, p. 1699-1706. <https://doi.org/10.1016/j.buildenv.2008.11.010>.

Hewett, Paul et Gary H. Ganser. 2017. « Models for nearly every occasion: Part I - One box models ». *Journal of Occupational and Environmental Hygiene*, vol. 14, nº 1, p. 49-57. <https://doi.org/10.1080/15459624.2016.1213392>.

Hidy, George. 2012. *Aerosols: An Industrial and environmental science*. Elsevier, 795 p.

Hilgenstock, A. et R. Ernst. 1996. « Analysis of installation effects by means of computational fluid dynamics—CFD vs experiments? » *Flow Measurement and Instrumentation*, vol. 7, nº 3, p. 161-171. <https://doi.org/10.1016/S0955-5986(97)88066-1>.

Hinds, William C. 1999. *Aerosol Technology: Properties, Behavior, and Measurement of Airborne Particles*. John Wiley & Sons, 504 p.

Hooff, T. et B. Blocken. 2012. « Full-scale measurements of indoor environmental conditions and natural ventilation in a large semi-enclosed stadium: Possibilities and limitations for CFD validation ». *Journal of Wind Engineering and Industrial Aerodynamics*, vol. 104-106, p. 330-341. <https://doi.org/10.1016/j.jweia.2012.02.009>.

Jayjock, M. A. 1997. « Modelling Inhalation Exposure ». *Di Nardi SR The Occupational Environment-its Evaluation and Control*.

Jensen, Alexander Christian Osterskov, Mikko Poikkimaki, Anders Brostrøm, Miikka Dal Maso, Ole John Nielsen, Thomas Rosenorn, Andrew Butcher, Ismo Kalevi Koponen et Antti Joonas Koivisto. 2019. « The effect of sampling inlet direction and distance on particle source measurements for dispersion modelling ». *Aerosol and Air Quality Research*, vol. 19, nº 5, p. 1114-1125.

Keil, Charles B., Catherine E. Cimmons et T. Renée Anthony, éd. 2009. *Mathematical models for estimating occupational exposure to chemicals*, 2nd edition. Fairfax, VA : American Industrial Hygiene Association, 207 p.

Kulkarni, Pramod, Paul A. Baron et Klaus Willeke, éd. 2011. *Aerosol Measurement: Principles, Techniques, and Applications*, 3 edition. Hoboken, N.J : Wiley, 900 p.

Lai, Alvin CK et William W. Nazaroff. 2000. « Modelling indoor particle deposition from turbulent flow onto smooth surfaces ». *Journal of aerosol science*, vol. 31, nº 4, p. 463-476.

Landrigan, Philip J., Richard Fuller, Nereus J. R. Acosta, Olusoji Adeyi, Robert Arnold, Niladri (Nil) Basu, Abdoulaye Bibi Baldé, Roberto Bertollini, Stephan Bose-O'Reilly, Jo Ivey Boufford, Patrick N. Breysse, Thomas Chiles, Chulabhorn Mahidol, Awa M. Coll-Seck, Maureen L. Cropper, Julius Fobil, Valentin Fuster, Michael Greenstone, Andy Haines, David Hanrahan, David Hunter, Mukesh Khare, Alan Krupnick, Bruce Lanphear, Bindu Lohani, Keith Martin, Karen V. Mathiasen, Maureen A. McTeer, Christopher J. L. Murray, Johanita D. Ndahimananjara, Frederica Perera, Janez Potočnik, Alexander S. Preker, Jairam Ramesh, Johan Rockström, Carlos Salinas, Leona D. Samson, Karti Sandilya, Peter D. Sly, Kirk R. Smith, Achim Steiner, Richard B. Stewart, William A. Suk, Onno C. P. van Schayck, Gautam N. Yadama, Kandeh Yumkella et Ma Zhong. 2018. « The Lancet Commission on pollution and health ». *The Lancet*, vol. 391, nº 10119, p. 462-512. <https://doi.org/10.1016/S0140-6736(17)32345-0>.

Liu, Xiaoran, Fei Li, Hao Cai, Bin Zhou, Shanshan Shi et Jinxiang Liu. 2019. « A numerical investigation on the mixing factor and particle deposition velocity for enclosed spaces under natural ventilation ». In *Building Simulation*. (2019), p. 465-473. Springer.

Logan, Perry, Gurumurthy Ramachandran, John Mulhausen et Paul Hewett. 2009. « Occupational Exposure Decisions: Can Limited Data Interpretation Training Help Improve Accuracy? » *The Annals of Occupational Hygiene*, vol. 53, nº 4, p. 311-324. <https://doi.org/10.1093/annhyg/mep011>.

Manigrasso, Maurizio, Carmela Protano, Matteo Vitali et Pasquale Avino. 2019. « Where do ultrafine particles and nano-sized particles come from? » *Journal of Alzheimer's Disease*, vol. 68, nº 4, p. 1371-1390.

May, K. R. 1973. « The collison nebulizer: Description, performance and application ». *Journal of Aerosol Science*, vol. 4, nº 3, p. 235-243. <https://doi.org/10.1016/0021-8502(73)90006-2>.

McGrattan, Kevin B, Howard R Baum, Ronald G Rehm, Anthony Hamins et Glenn P Forney. 2021. « Fire dynamics simulator: technical reference guide ». p. 41.

Minier, Jean-Pierre et Jacek Pozorski. 2017. *Particles in wall-bounded turbulent flows: deposition, re-suspension and agglomeration*. Springer.

Mølgaard, Bjarke, Jakub Ondráček, Petra Št´ávová, Lucie Džumbová, Martin Barták, Tareq Hussein et Jiří Smolík. 2014. « Migration of aerosol particles inside a two-zone apartment with natural ventilation: A multi-zone validation of the multi-compartment and size-resolved indoor aerosol model ». *Indoor and Built Environment*, vol. 23, nº 5, p. 742-756. <https://doi.org/10.1177/1420326X13481484>.

Nerisson, Philippe. 2009. « Modélisation du transfert des aérosols dans un local ventilé ». phd. <http://ethesis.inp-toulouse.fr/archive/00000727/>.

Newman, Perry A. et Institute for Computer Applications in Science and Engineering. 1996. *Observations Regarding Use of Advanced CFD Analysis, Sensitivity Analysis, and Design Codes in MDO*. Institute for Computer Applications in Science and Engineering, NASA Langley Research Center, 24 p.

NIOSH. 2013. « CDC - Skin Exposures and Effects - NIOSH Workplace Safety and Health Topic ». <https://www.cdc.gov/niosh/topics/skin/default.html>.

Ribalta, Carla, Antti J. Koivisto, Ana López-Lilao, Sara Estupiñá, María C. Minguillón, Eliseo Monfort et Mar Viana. 2019. « Testing the performance of one and two box models as tools for risk assessment of particle exposure during packing of inorganic fertilizer ». *Science of The Total Environment*, vol. 650, p. 2423-2436. <https://doi.org/10.1016/j.scitotenv.2018.09.379>.

Ribalta, Carla, Antti J. Koivisto, Apostolos Salmatonidis, Ana López-Lilao, Eliseo Monfort et Mar Viana. 2019. « Modelling of high nanoparticle exposure in an indoor industrial scenario with a one-box model ». *International journal of environmental research and public health*, vol. 16, nº 10, p. 1695.

Ribalta, Carla, Ana López-Lilao, Ana Sofia Fonseca, Alexander Christian Østerskov Jensen, Keld Alstrup Jensen, Eliseo Monfort et Mar Viana. 2021. « Evaluation of One- and Two-Box Models as Particle Exposure Prediction Tools at Industrial Scale ». *Toxics*, vol. 9, nº 9, p. 201. <https://doi.org/10.3390/toxics9090201>.

Rim, Donghyun, Michal Green, Lance Wallace, Andrew Persily et Jung-Il Choi. 2012. « Evolution of Ultrafine Particle Size Distributions Following Indoor Episodic Releases: Relative Importance of Coagulation, Deposition and Ventilation ». *Aerosol Science and Technology*, vol. 46, nº 5, p. 494-503. <https://doi.org/10.1080/02786826.2011.639317>.

Robinson, Gary, Robert Michaels, Laurence Britton, Lance Edwards, Richard Gowland, Ronald Keefer, Ron Kirsch, Arthur Krawetz, F. Kubias, Roland Land, Kenneth Lewis, David Peterson, William Satterfield, David Wechsler, Ira Wainless, Amy Spencer, Ira Wainless et Amy Spencer. 2006. *NFPA 704, 2007 Edition, Standard System for the Identification of the Hazards of Materials for Emergency Response.* <https://doi.org/10.13140/RG.2.2.32358.01608>.

Saidi, M. N., V. Songmene, J. Kouam et A. Bahloul. 2015. « Experimental investigation on fine particle emission during granite polishing process ». *The International Journal of Advanced Manufacturing Technology*, vol. 81, nº 9, p. 2109-2121. <https://doi.org/10.1007/s00170-015-7303-z>.

Soltani, Mehdi et Goodarz Ahmadi. 1999. « Charged Particle Trajectory Statistics and Deposition in a Turbulent Channel Flow ». *Aerosol Science and Technology*, vol. 31, nº 2-3, p. 170-186. <https://doi.org/10.1080/027868299304228>.

Thurston, George D., Howard Kipen, Isabella Annesi-Maesano, John Balmes, Robert D. Brook, Kevin Cromar, Sara De Matteis, Francesco Forastiere, Bertil Forsberg, Mark W. Frampton, Jonathan Grigg, Dick Heederik, Frank J. Kelly, Nino Kuenzli, Robert Laumbach, Annette Peters, Sanjay T. Rajagopalan, David Rich, Beate Ritz, Jonathan M. Samet, Thomas Sandstrom, Torben Sigsgaard, Jordi Sunyer et Bert Brunekreef. 2017. « A joint ERS/ATS policy statement: what constitutes an adverse health effect of air pollution? An analytical framework ». *European Respiratory Journal*, vol. 49, nº 1. <https://doi.org/10.1183/13993003.00419-2016>.

Vadali, Monika, Gurumurthy Ramachandran, John R Mulhausen et Sudipto Banerjee. 2012. « Effect of Training on Exposure Judgment Accuracy of Industrial Hygienists ». *Journal of Occupational and Environmental Hygiene*, vol. 9, nº 4, p. 242-256. <https://doi.org/10.1080/15459624.2012.666470>.

Van Landuyt, Kirsten L., Bryan Hellack, Bart Van Meerbeek, Marleen Peumans, Peter Hoet, M. Wiemann, T. A. J. Kuhlbusch et C. Asbach. 2014. « Nanoparticle release from dental composites ». *Acta Biomaterialia*, vol. 10, nº 1, p. 365-374.

Viitanen, Anna-Kaisa, Sanni Uuksulainen, Antti J. Koivisto, Kaarle Hämeri et Timo Kauppinen. 2017. « Workplace measurements of ultrafine particles—a literature review ». *Annals of Work Exposures and Health*, vol. 61, nº 7, p. 749-758.

Wu, C. Y., Y. M. Ferng, C. C. Chieng et C. C. Liu. 2010. « Investigating the advantages and disadvantages of realistic approach and porous approach for closely packed pebbles in CFD simulation ». *Nuclear Engineering and Design*, vol. 240, nº 5, p. 1151-1159. <https://doi.org/10.1016/j.nucengdes.2010.01.015>.

Zahmatkesh, Iman. 2008. « On the importance of thermophoresis and Brownian diffusion for the deposition of micro- and nanoparticles ». *International Communications in Heat and Mass Transfer*, vol. 35, nº 3, p. 369-375. <https://doi.org/10.1016/j.icheatmasstransfer.2007.08.004>.

Zhang, Meibian, Le Jian, Pingfan Bin, Mingluan Xing, Jianlin Lou, Liming Cong et Hua Zou. 2013. « Workplace exposure to nanoparticles from gas metal arc welding process ». *Journal of nanoparticle research*, vol. 15, nº 11, p. 2016.

Zuskin, E., J. Mustajbegovic, E. N. Schachter, D. Pavicic et A. Budak. 1997. « A follow-up study of respiratory function in workers exposed to acid aerosols in a food-processing industry ». *International Archives of Occupational and Environmental Health*, vol. 70, nº 6, p. 413-418. <https://doi.org/10.1007/s004200050238>.